# Absolute Paleolatitude of Northern Zealandia From the Middle Eocene to the Early Miocene

Edoardo Dallanave[1] [ID], Rupert Sutherland[2] [ID], Gerald R. Dickens[3] [ID], Liao Chang[4] [ID], Evdokia Tema[5] [ID], Laia Alegret[6] [ID], Claudia Agnini[7] [ID], Thomas Westerhold[8] [ID], Cherry Newsam[9,10], Adriane R. Lam[11] [ID], Wanda Stratford[12] [ID], Julien Collot[13] [ID], Samuel Etienne[13] [ID], and Tilo von Dobeneck[1] [ID]

[1]Faculty of Geosciences, University of Bremen, Bremen, Germany, [2]School of Geography, Environment and Earth Sciences, Victoria University of Wellington, Wellington, New Zealand, [3]Department of Geology, Trinity College Dublin, Dublin, Ireland, [4]School of Earth and Space Sciences, Peking University, Beijing, China, [5]Department of Earth Sciences, University of Turin, Turin, Italy, [6]Universidad de Zaragoza & Instituto Universitario de Ciencias Ambientales, Zaragoza, Spain, [7]Department of Geosciences, University of Padova, Padova, Italy, [8]MARUM, University of Bremen, Bremen, Germany, [9]University College London, London, UK, [10]Now at Network Stratigraphic Consulting Ltd, Potters Bar, UK, [11]Department of Geological Sciences and Environmental Studies, Binghamton University, SUNY, Binghamton, NY, USA, [12]GNS Sciences, Lower Hutt, New Zealand, [13]Service de la Géologie de Nouvelle Calédonie, Direction de l'Industrie, des Mines et de l'Energie de Nouvelle Calédonie, Nouméa, New Caledonia

**Abstract** The absolute position during the Cenozoic of northern Zealandia, a continent that lies more than 90% submerged in the southwest Pacific Ocean, is inferred from global plate motion models, because local paleomagnetic constraints are virtually absent. We present new paleolatitude constraints using paleomagnetic data from International Ocean Discovery Program Site U1507 on northern Zealandia and Site U1511 drilled in the adjacent Tasman Sea Basin. After correcting for inclination shallowing, five paleolatitude estimates provide a trajectory of northern Zealandia past position from the middle Eocene to the early Miocene, spanning geomagnetic polarity chrons C21n to C5Er (~48–18 Ma). The paleolatitude estimates support previous works on global absolute plate motion where northern Zealandia migrated 6° northward between the early Oligocene and early Miocene, but with lower absolute paleolatitudes, particularly in the Bartonian and Priabonian (C18n–C13r). True polar wander (solid Earth rotation with respect to the spin axis), which only can be resolved using paleomagnetic data, may explain the discrepancy. This new paleomagnetic information anchors past latitudes of Zealandia to Earth's spin axis, with implications not only for global geodynamics, but also for addressing paleoceanographic and paleoclimate problems, which generally require precise paleolatitude placement of proxy data.

**Plain Language Summary** The ancient latitude (paleolatitude) of a tectonic plate can be determined from magnetism recorded in rocks (paleomagnetism). Earth's geomagnetic field, averaged over geological time, is symmetrical around Earth's spin axis. Hence, the direction of the remanent magnetization in rocks can provide the paleolatitude and orientation of a tectonic plate with respect to the geographic poles. Using marine sediments recovered during International Ocean Discovery Program Expedition 371, we present five paleolatitude estimates for northern Zealandia, a mostly submerged continent in the southwest Pacific encompassing New Zealand and New Caledonia. The reconstructed paleolatitudes span the time interval from 48 to 18 million years ago (middle Eocene to middle Miocene), and represent the first such estimates from northern Zealandia. Geodynamic models for Earth surface motion relative to the spin axis require several assumptions and do not accurately predict our results. Combined with data from other continents, a more precise reconstruction for Zealandia's past geography has implications for understanding various fossil records in this extensive region, including those important for past ocean circulation and climate models, and for the evolution of plants and animals.

## 1. Introduction

Zealandia, a mostly submerged continent covering $4.9 \times 10^6$ km$^2$ in the southwest Pacific (Mortimer et al., 2017), sits astride two tectonic plates separated by an active plate boundary: northern Zealandia lies on the Australian Plate, while southern Zealandia lies on the Pacific Plate (Figure 1). While the islands of New Zealand and New

Tema, Laia Alegret, Claudia Agnini, Thomas Westerhold, Cherry Newsam, Adriane R. Lam, Wanda Stratford, Julien Collot, Samuel Etienne, Tilo von Dobeneck

**Writing – review & editing:** Rupert Sutherland, Gerald R. Dickens, Evdokia Tema, Laia Alegret, Claudia Agnini, Thomas Westerhold, Cherry Newsam, Adriane R. Lam, Wanda Stratford, Julien Collot, Samuel Etienne, Tilo von Dobeneck

Caledonia emerge above present-day sea level, about 94% of Zealandia sits underwater with an average water depth of about 1,100 m, an atypical hypsometry that relates to a relatively thin average continental crust thickness of ∼18 km (Hackney et al., 2012; Klingelhoefer et al., 2007; Sutherland et al., 2010). The oceanic crust of the Tasman Sea Basin, where seafloor spreading occurred for about 30 Myr between the late Cretaceous and early Eocene (83–53 Ma; Gaina et al., 1998), separates the continents of Zealandia and Australia.

The tectonic history of northern Zealandia during the Cenozoic is largely modulated by changes in relative motion between the Australian and Pacific plates (Cluzel et al., 2012; Collot et al., 2020; Matthews et al., 2015; Sutherland et al., 2020). Currently, the Pacific Plate subducts westward beneath the Tonga-Kermadec (T-K) Arc (Figure 1). However, during the early to middle Eocene and after cessation of Tasman seafloor spreading, T-K subduction initiated proximal to Norfolk Ridge (Gurnis et al., 2004), the northernmost part of which emerges as New Caledonia (Cluzel et al., 2012; Collot et al., 2020; Sutherland et al., 2020). Marked variations in the lithology and accumulation rates of Paleogene sediments presently exposed in New Zealand and New Caledonia reveal that significant tectonic change occurred around 46–44 Ma (Bordenave et al., 2021; Dallanave, Agnini, et al., 2018; Dallanave et al., 2015, 2020; Maurizot, 2011; Maurizot & Cluzel, 2014), attributed to early T-K subduction and uplift of northern Zealandia (Dallanave et al., 2020).

International Ocean Discovery Program (IODP) Expedition (Exp.) 371 aimed to better constrain the timing and dynamics of northern Zealandia paleogeography during the Cenozoic (Sutherland et al., 2018, 2019b). A total of 2,506 m sediments and volcanic rocks were recovered from cores drilled at six sites (Figure 1) with the scientific drillship *JOIDES Resolution* (JR). Five sites were drilled into sediments on the continental crust of northern Zealandia (Sites U1506–U1510) and one was drilled into sediments overlying oceanic crust in the eastern Tasman Abyssal Plain (Site U1511). Sediments recovered during Exp. 371 reveal a complex tectonic history of vertical motion across northern Zealandia, starting in the early Eocene (∼50 Ma) and continuing throughout much of the Cenozoic; deformation generally progressed from north to south (Sutherland et al., 2020). Sedimentary record from Exp. 371 gives important information about the tectonic and paleoenvironmental evolution for the Tasman area (Alegret et al., 2021; Stratford et al., 2022; Sutherland et al., 2022), and here we also use it to constrain the absolute paleoposition of northern Zealandia during the Cenozoic. Accurate paleogeography is essential for understanding past climate dynamics (e.g., Donnadieu et al., 2006), the paleogeographic distribution of fossils (e.g., Lam et al., 2018, 2021; Middlemiss, 1979), and the absolute positions of land and ocean to constrain paleoclimate models (Herold et al., 2008; Hollis et al., 2019; Lunt et al., 2017).

Paleolatitude estimates for northern Zealandia through the Cenozoic are uncertain because no autochthtonous paleomagnetic constraints exist, and the bordering Australian Plate has very limited data (Dallanave & Kirscher, 2020; Hansma & Tohver, 2019). At present, the paleogeographic position of Zealandia is determined via data from connected plates by means of absolute plate motion (APM) models. An APM model is built from a relative plate motion (RPM) model, which describes the rotation of all tectonic plates relative to each other through analysis of seafloor magnetic anomalies and fracture zones (Müller et al., 2016, 2019). The APM model develops by anchoring the RPM model to a reference frame that does not change over geological time (Seton et al., 2012; Tetley et al., 2019; Torsvik et al., 2008). The two common reference frames adopted are the Earth's mantle and the spin axis. While the first mainly arises from analyses of hotspot tracks, the spin axis reference frame derives from paleomagnetism (Torsvik et al., 2008, 2012). Paleomagnetic directions measured at a given locality result in a paleomagnetic pole, which virtually coincides with the paleoposition of the Earth's spin axis relative to the sampling site (Dallanave & Kirscher, 2020; Tauxe, 2010; Vaes et al., 2021). Compilations of consecutive poles then are combined to establish an apparent polar wander path (APWP, called apparent because it rather reflects the changing orientation and distance of the plate with respect the geographic pole; Besse & Courtillot, 2002; Creer et al., 1954; Torsvik et al., 2008; Van der Voo, 1993). However, the Cenozoic paleomagnetic data set used to create the global APWP is strongly biased by data from the North American continent. Examination of middle Eocene to the early Miocene (48–18 Ma; Chrons C21n–C5En) paleomagnetic entries compiled by Torsvik et al. (2012), which we integrate here with Australian entries presented by Hansma and Tohver (2019), reveals that 18 paleomagnetic poles out of 42 (∼43%) are from North America, and the other 23 poles are distributed among the other continents (Table S1). Sites drilled during IODP Exp. 371 provide an excellent opportunity to test if currently referenced APM models predict an accurate paleogeography for northern Zealandia.

Here, we present a set of five paleolatitudes for northern Zealandia between the middle Eocene and early Miocene. Paleolatitudes are determined from paleomagnetic inclination of sediments recovered at Sites U1507 and U1511
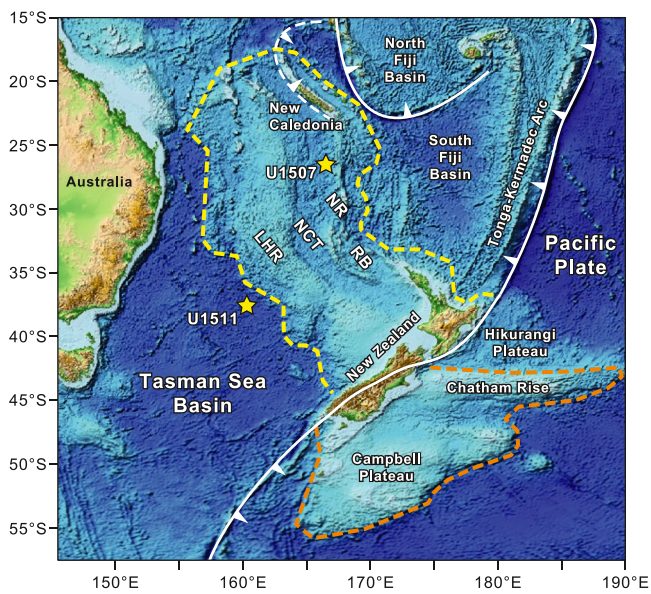
**Figure 1.** Present-day map of northern (enveloped by the yellow dashed line) and southern (enveloped by the orange dashed line) Zealandia, with yellow stars indicating the location of International Ocean Discovery Program Sites U1507 (26.4886°S, 166.5286°E) and U1511 (37.5611°S, 160.3156°E). Solid and dashed white lines indicate active and inactive subduction zones, respectively, with arrows lying on the overriding plate. LHR = Lord Howe Rise, NCT = New Caledonia trough, NR = Norfolk Ridge, RB = Reinga basin.

(Figures 1 and 2), after correction for inclination shallowing (Collombat et al., 1993; Hodych et al., 1999). Although Site U1511 was drilled on the oceanic crust of Tasman Abyssal Plain, paleolatitudes determined here represent those of northern Zealandia, because this part of the Tasman Sea connects to the Lord Howe Rise via a passive margin (Figure 1).

## 2. Sites, Lithostratigraphy, and Previous Work

### 2.1. Hole U1507B

Hole U1507B (26.4886°S, 166.5286°E) was drilled on the eastern side of New Caledonia Trough at 3,568 m water depth (Figure 1). The hole extends from 376 to 864 m below the sediment-water interface (here and after, core depths are expressed on a core depth below sea floor meter scale—CSF-A—as determined on ship; https://www.iodp.org/policies-and-guidelines). Sediments were retrieved using the rotary core barrel (RCB) technique, with a total core recovery of 76%. They consist of clayey calcareous chalk with volcanic material from the top of the hole down to Core 35R at 685 m, and calcareous chalk from this depth to Core 52R at 855.6 m. The age of the sediments cored at Hole U1507B spans from the middle Eocene to the early Miocene, as determined by biostratigraphy and magnetostratigraphy, and it correlates with Chrons C5–C18 (Figure 2a).
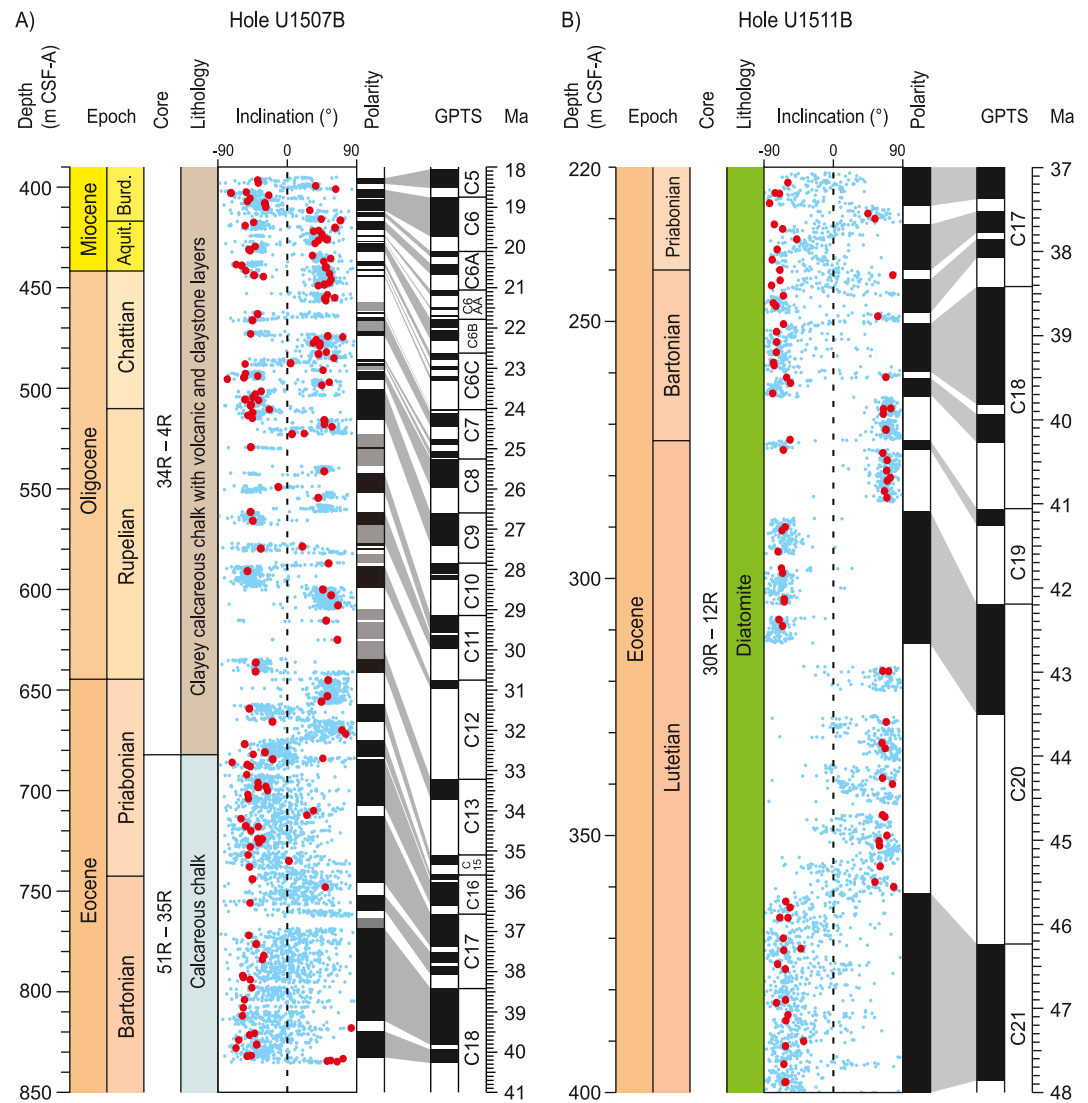
### 2.2. Hole U1511B

Hole U1511B (37.5611°S, 160.3156°E) was drilled on Tasman Sea Abyssal Plain near the western margin of Lord Howe Rise at 4,847 m water depth (Figure 1). The hole extends from 19.8 to 566.2 m (Core 2R to Core 47R). The interval between 77.2 and 192.2 m was drilled without recovery ("washed"), in order to accelerate collection of deeper strata with primary significance to expedition objectives. Sediments were retrieved using the RCB technique, with a total of 65% recovery. Greenish gray to yellowish brown diatomite and claystone were recovered from Core 10R to Core 30R (201.9–403.4 m), overlying red to greenish gray claystone (up to Core 43R at 560.7 m) (Sutherland et al., 2019d). The age of the sediments drilled at Hole U1511B ranges from Pleistocene to lower Paleocene, as determined by biostratigraphy and magnetostratigraphy (Sutherland et al., 2019d). The part of the hole relevant to this work, between Core 12R and Core 30R (high quality paleomagnetic signal), correlates with Chrons C17n–C21n, from the uppermost early Eocene to the lowermost late Eocene (Figure 2b).

### 2.3. Published Paleomagnetic Data

All sediment cores retrieved from boreholes during Exp. 371 were cut into sections (typically 1.5 m in length) and subsequently split longitudinally on board the JR into working and archive halves. Following standard shipboard procedures (Sutherland et al., 2019a), the natural remanent magnetization (NRM) of core archive halves was demagnetized with an alternating magnetic field (AF) up to 20 mT. NRM inclination after 20 mT demagnetization is used as base for determining the series of paleomagnetic reversals through the records for correlation with the geomagnetic polarity time scale (GPTS) (Figure 2). The above shipboard data was supplemented with paleomagnetic information obtained from fully demagnetized discrete specimens collected initially onboard the JR and after, during the sampling party, at the IODP Gulf Coast Core Repository (College Station, TX, USA). These samples (~8 cm$^3$ cubes) were trimmed directly from lithified sediments of the working halves, and additional data were generated as follows.

For Hole U1507B, 72 discrete samples were collected and measured on board the JR using seven AF demagnetization steps up to a maximum of 70 mT (or up to 90 mT in some few cases). The remanence was measured with an AGICO JR-6 Spinner Magnetometer. To refine the magnetostratigraphic control, during the post-cruise sampling party we collected a total of 151 from the two intervals between cores 4–17R and 32–52R. A set of 74 samples from these was processed by applying 15 AF demagnetization steps up to 100 mT. The remanence

**Figure 2.** Lithology, magnetic polarity stratigraphy and age of sediment cored at (a) Hole U1507B and (b) Hole U1511B. Blue dots are paleomagnetic inclinations determined by shipboard measurement of the archive half after 20 mT alternating field magnetic cleaning. Red dots are paleomagnetic directions derived from discrete specimens measured during either Exp. 371 or a post-cruise analysis phase. Data presented by Sutherland et al. (2019a, 2019c) and Dallanave and Chang (2020) are here correlated with the geomagnetic polarity time scale (GPTS) of Westerhold et al. (2020).

was measured automatically after each step with an in-line 2G Enterprises superconducting rock magnetometer at the paleomagnetic laboratory of the University of Bremen (Mullender et al., 2016). Within some specific stratigraphic intervals, the AF protocol resulted in a characteristic remanent magnetization (ChRM) direction failing to point toward the origin of the demagnetization axes. Therefore, for other 72 specimens, we applied stepwise thermal demagnetization up to 600°C to using a Schönstedt thermal demagnetizer, measuring the remanence after each demagnetization step with a 2G Enterprises superconducting rock magnetometer (Dallanave & Chang, 2020).

For Hole U1511B, quasi-continuous shipboard NRM measurements on the archive half (after 20 mT AF cleaning) were integrated with data from 33 discrete specimens demagnetized with AF protocol up to 120 mT. To refine the magnetostratigraphic control, during the post-cruise sampling party we selected 105 cube specimens of 8 cm³ volume from cores 12R–30R. The shipboard AF procedure was not always sufficient to fully demagnetize the samples, so we selected 60 specimens (from the 105) to analyze with stepwise thermal demagnetization up to 650°C. Thermal demagnetization was performed with a Schönstedt paleomagnetic furnace, measuring the

remanence after each step with a 2G Enterprises cryogenic magnetometer (Dallanave & Chang, 2020). The remaining cube samples were used for rock-magnetic analyses or stored as archive.

## 3. New Data and Paleomagnetic Analyses

### 3.1. Paleomagnetic Directions

Integration of paleomagnetic data from shipboard (Sutherland et al., 2019c, 2019d) and shore-based analyses (Dallanave & Chang, 2020) provides well defined paleomagnetic directions for the sedimentary records of Holes U1507B and U1511B. When combined with biostratigraphic information (Sutherland et al., 2019c, 2019d), straightforward correlations to the GPTS can be made (Figure 2). Because paleolatitude estimation requires paleomagnetic directions representative of the geomagnetic field, for this work we used only data from fully demagnetized discrete specimens.

Although the sampling resolution of Hole U1507B allows for sufficient correlation to the GPTS, additional samples were needed for precise paleolatitude estimates. To increase the paleomagnetic data set for this work, we requested from the Kochi Core Center (Nankoku, Japan) further 67 oriented specimens from Hole U1507B, 41 of which were from cores 18R–30R, and 26 were from cores 31R–50R. These were all subjected to AF demagnetization with 17 steps between 3 and 100 mT at the University of Bremen. Thus, in total, 306 discrete sediment samples were demagnetized for paleomagnetic direction analysis: 213 from Hole U1507B and 93 from Hole U1511B.

To improve the quality of the directional data set, all data from the 306 AF and thermally demagnetized specimens were inspected using stricter statistical criteria than previously used by Dallanave and Chang (2020). Specifically, we investigated the NRM behavior through visual inspection of vector end-point diagrams (Zijderveld, 1967) using the PuffinPlot open source software (Lurcock & Wilson, 2012). The ChRM of each specimen was isolated applying principal component analysis on the selected vector end-points as proposed by Kirschvink (1980). We applied two selection criteria: (a) minimum of five vector end-points and (b) maximum angular deviation (MAD, Kirschvink, 1980) lower than 10°. When using principal component analysis for estimating ChRM directions, it is a common practice to force the direction to pass through the origin of the demagnetization axes when it visually trends toward it. This procedure, referred to as "anchoring," may result in artificially low MAD estimation. To maximize the reliability of our directions, we adopted the Bayesian model techniques developed by Heslop and Roberts (2016) to assess whether anchoring each ChRM was statistically justifiable or not. Heslop and Roberts (2016) also propose a new computational strategy to fit vectors that are constrained to pass through the vector demagnetization diagram origin and provides more realistic ChRM vector directions and associated MAD. These directions are defined as "constrained" (please refer to Heslop & Roberts, 2016 for details).

The RCB technique results in cores with unknown azimuth. Hence, the paleomagnetic declination is undefined, and the average paleomagnetic direction of a set of samples cannot be calculated using standard spherical statistics (Fisher, 1953). We estimated the average inclination of set of directions by adopting the maximum likelihood solution for inclination data, an approach presented by Arason and Levi (2010). This method minimizes the shallow-biased error that can occur when calculating mean inclination in the absence of declination data. The obtained paleomagnetic inclination can be converted to paleolatitude and paleo-colatitdue by using the geocentric axial dipole tangent function (Tauxe, 2010):

$$\tan I = 2 \tan \lambda \tag{1}$$

where $I$ is the paleomagnetic inclination and $\lambda$ is the paleolatitude. Colatitude is defined the difference between 90° and the latitude.

### 3.2. Rock-Magnetism and Paleomagnetic Inclination Flattening

The behavior of specimens monitored during AF and thermal demagnetization already provides insight into the nature of NRM carriers. To better characterize the magnetic mineralogy, 20 representative specimens (10 from each hole) were subjected to stepwise isothermal remanent magnetization (IRM) acquisition up to 700 mT, and the IRM was measured automatically after each step (Mullender et al., 2016). For sediments recovered from Hole U1511B, this field was often insufficient to reach magnetic remanence saturation, so we completed the analysis

by stepwise magnetizing the specimens manually up to a field of 2.5 T, measuring their IRM after each step. The resulting IRM curves were "unmixed" for their coercivity components by means of skewed generalized Gauss distribution (Egli, 2003) using the RStudio-based MAX UnMix code (Maxbauer et al., 2016).

The paleomagnetic data set from holes U1507B and U1511B in this work is used for paleolatitude calculation. Hence, it is fundamental to detect and correct for paleomagnetic inclination shallowing, otherwise uncorrected data can misplace paleolatitudes by several degrees (Tauxe et al., 2008). In order to detect and estimate the degree of inclination shallowing there are two families of methods. The first is based on the shape of paleomagnetic direction distribution that is, for a given locality, compared with the one expected from the paleosecular variations model (Tauxe & Kent, 2004). This method has been successfully applied to a wide variety of sedimentary rocks (e.g., Dallanave, Agnini, et al., 2012; Dallanave, Muttoni, et al., 2012; Dallanave, Kirscher, et al., 2018; Dallanave et al., 2009; Kent & Tauxe, 2005; Kirscher et al., 2014; Krijgsman & Tauxe, 2006). However, it requires an adequate number of directions with well-defined inclination and declination, of which the latter is often absent (or not sufficiently accurate) in paleomagnetic data obtained from deep-sea cores. The second family of methods is based on the quantification of magnetic fabric, in the form of either anisotropy of magnetic susceptibility (AMS), anisotropy of anhysteretic remanent magnetization (AARM), or anisotropy of IRM (e.g., Bilardello, 2015; Bilardello & Kodama, 2010; Bilardello et al., 2011; Kodama & Sun, 1992; Tan & Kodama, 2003). In our work, we detected and corrected for paleomagnetic inclination shallowing by exploring the partial AARM (Site U1507) and its behavior during AF demagnetization, and the anisotropy of IRM (Site U1511) and its behavior during thermal demagnetization. The analytical procedure is extensively discussed in Sections 1 and 2 of the Supporting Information S1.

The degree of paleomagnetic direction flattening determined for the sediments was used to correct the measured ChRM inclination by applying the tangent function introduced by King (1955):

$$\tan I_o = f \cdot \tan I_f \qquad (2)$$

where $I_o$ and $I_f$ are the observed NRM inclination and the original geomagnetic field inclination, respectively, and $f$ is the flattening factor that ranges from 0 (completely flattened directions) to 1 (absence of flattening).

## 4. Results

### 4.1. Rock-Magnetism and Paleomagnetism of Hole U1507B

The magnetic minerals of specimens from Hole U1507B are dominated by a low coercivity phase interpreted as magnetite. During AF demagnetization, the decay in NRM intensity can be used to calculate a median destructive field (i.e., the field at which half of the NRM is lost). The average median destructive field is 28 mT and >90% of NRM is removed after a 100 mT AF (Figure 3a). This is in agreement with the averaged median destructive field of ARM (applied with an AF of 100 mT and a direct current field of 0.1 mT; Section 1 of Supporting Information S1), which is 31 mT (inset in Figure 3a), and consistent with the presence of magnetite as the main magnetic carrier (e.g., Frank & Nowaczyk, 2008). IRM acquisition curves are dominated by a low coercivity component with a $B_{1/2}$ (the field required to reach half of the saturation) of ~60 mT (Figures 3b and 3c), similar to those reported for sediments with NRM carried by magnetite (e.g., Dallanave et al., 2015).

By inspection of all the demagnetization data of the specimens measured during IODP Exp. 371 and post-expedition, we isolated a total of 165 high-quality ChRM directions (Figure 4a). They have been estimated by interpolating on average 10 vector end-points, only 11 of them are anchored to the origin of the demagnetization axes, 31 are constrained, and the remaining 123 are not-anchored. The average MAD of 3.4° is indicative of the quality of the data set (Table S2). The normal and reversed polarity directions (after correction for inclination shallowing) are statistically undistinguishable at a 95% confidence level, excluding the presence of a pervasive and unresolved paleomagnetic overprint (Table 1). Analogously, when calculating the average inclination of thermally and AF demagnetized specimens (plotted on a common down-pointing polarity), the mean values are statistically undistinguishable at a 95% confidence level. This indicates that both techniques give comparable results. On average, the number of paleomagnetic directions falling within the reliability criteria is higher in clayey chalk than in calcareous chalk. This is shown by an average MAD of 3.0° for samples from the first lithology compared to an average MAD of 5.2° in samples from the latter lithology. This likely results from the significant difference in NRM intensity (Figure 4b).
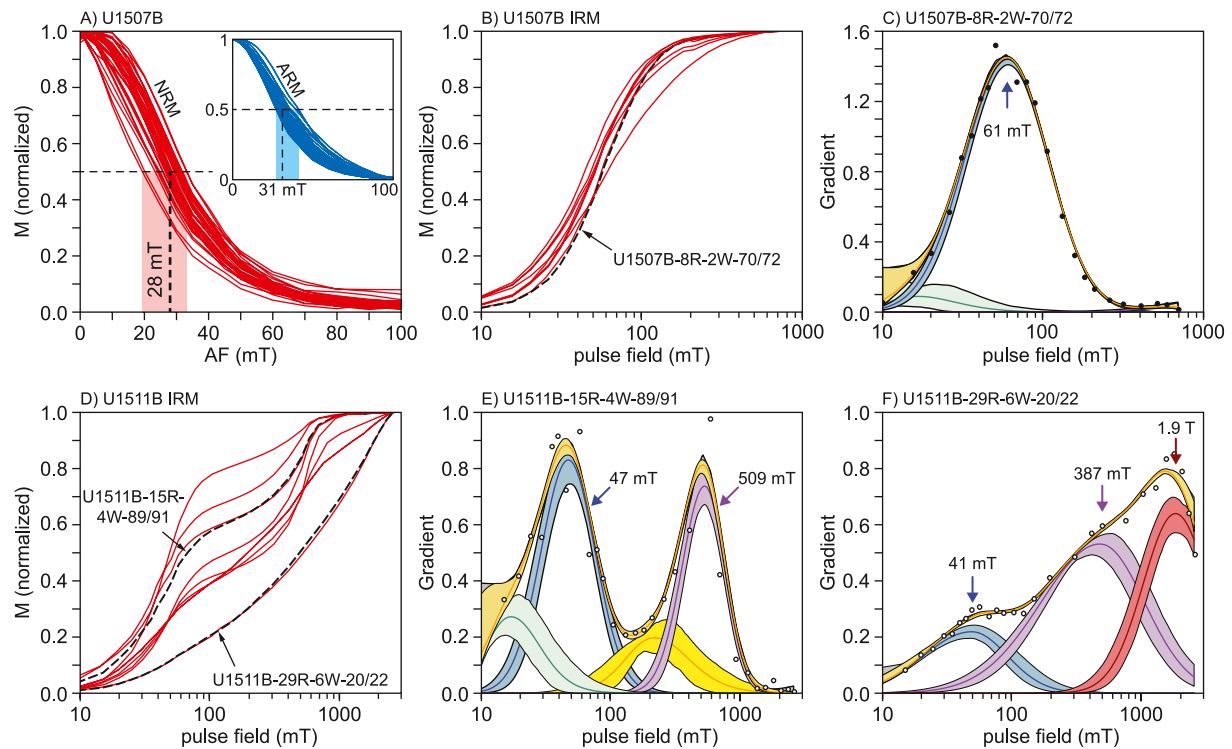
**Figure 3.** Rock-magnetic analyses. (a) Decay during alternating field demagnetization of the natural remanent magnetization (NRM) for 33 selected specimens and anhysteretic remanent magnetization (ARM; inset) of 52 specimens from Hole U1507B, with indication of the averaged median destructive field. (b) Isothermal remanent magnetization (IRM) acquisition of 10 samples from Hole U1507B. (c) IRM component "unmixing" (see main text) for sample U1507B-8R-2W-70/72, the dashed line shown in panel (b). (d) IRM acquisition of 10 samples from Hole U1511B. (e–f) IRM component "unmixing" of samples U1511B-15R-4W-89/91 and U1511B-29R-6W-20/22, the dashed lines shown in panel (d). For the "unmixing" curves, the gray dots are the first derivative of the corresponding IRM curve, and the colored lines are the different modeled components, with indication of the $B_{1/2}$ (the field required to reach half of the saturation) of the dominant ones. The colored bands associated with the lines are the 95% confidence boundaries calculated from 100 bootstrapped data set (see Maxbauer et al., 2016 for details).

The estimated *f* values range from 0.74 to 0.99 (Figure 5, Table S2), with lower values in clayey chalk, as expected in sediments containing clay minerals. These flattening factors are generally similar to those found in the literature, measured with different methods on similar sedimentary rocks (see compilation of Muttoni et al., 2013). To correct the paleomagnetic inclination, we applied Equation 2 to each ChRM direction using *f* values as shown in Figure 5. Before correction, all directions were plotted as "down-pointing." With the downhole transition to calcareous chalk, from Core 34 down to Core 51, the measured flattening factor does not show significant variation, so we applied a blanket average *f* of 0.95 to all 40 directions.

### 4.2. Rock-Magnetism and Paleomagnetism of Hole U1511B

Rock-magnetic analyses indicate the presence of two magnetic coercivity phases within the Eocene diatomite of Hole U1511B. IRM acquisition curves (Figure 3d) show a low coercivity magnetic phase that reaches half of saturation at about 45 mT and a high coercivity magnetic phase that reaches half saturation at about 500 mT (Figure 3e). The proportion of these coexisting phases varies with depth. From Core 12R to Core 24R, the presence of dominant low coercivity magnetic phase and the maximum unblocking temperature of the ChRM direction below 600°C (Figure 4a) suggest magnetite as magnetization carrier (Dunlop & Özdemir, 1997). By contrast, high coercivity magnetic minerals dominate samples from cores 25R and 30R, the lowermost part of the studied interval (Figure 3f; Unit II of Sutherland et al., 2019a). Indeed, the IRM curves do not approach saturation even with applied magnetic field of ~2.5 T. This high coercivity, associated with a maximum unblocking temperature of the ChRM directions that reach 650°C (Figure 4a), suggest that between cores 25R and 30R the magnetization is carried by hematite (O'Reilly, 1984). Results of thermal demagnetization of IRM, used for estimating the degree of paleomagnetic inclination flattening, support this interpretation (Section 2 of the Supporting Information S1).
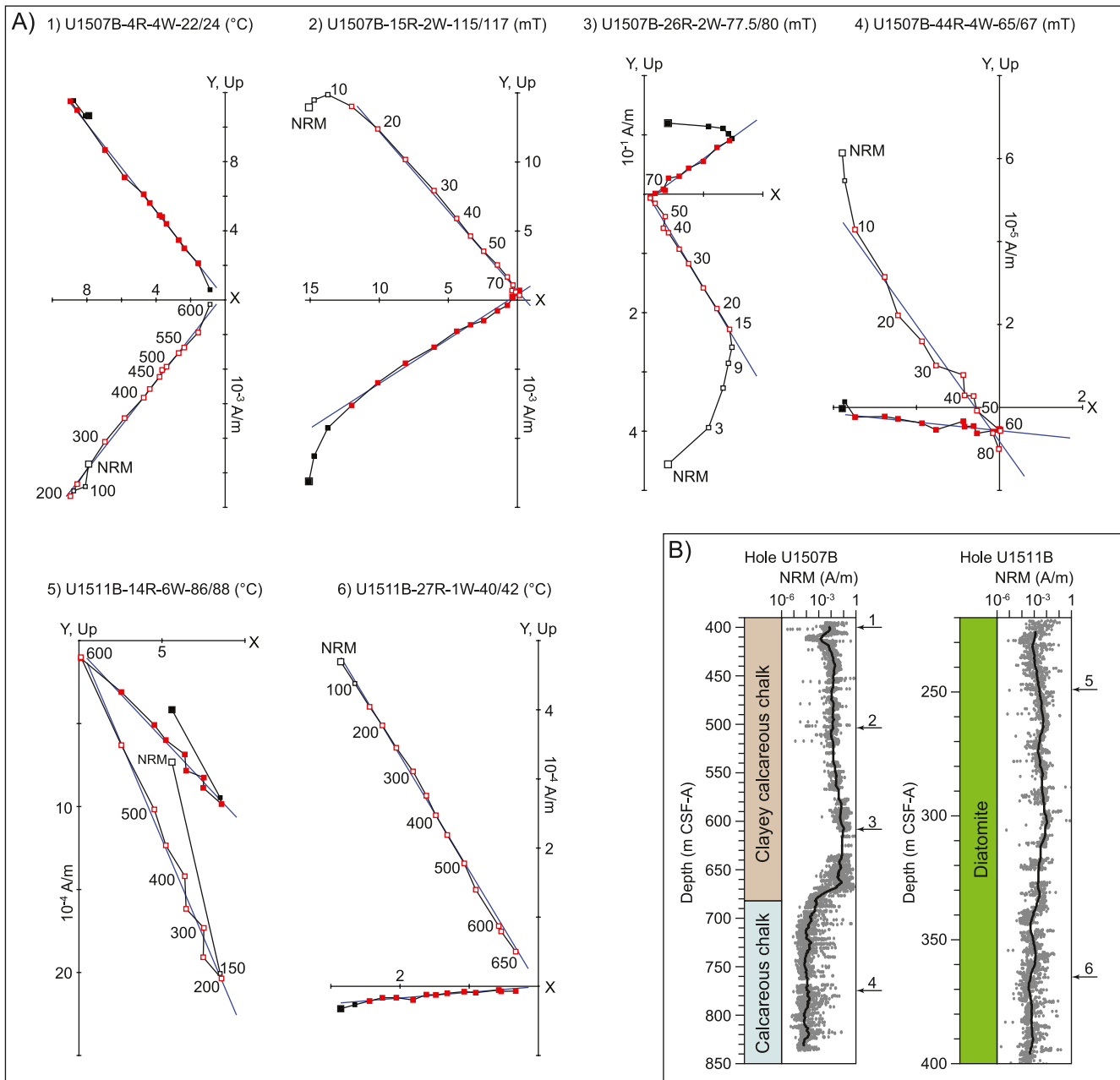
**Figure 4.** (a) Representative vector-end point demagnetization diagrams from Hole U1507B (1–4) and Hole U1511B (5–6); solid (open) squares are projections onto the vertical (horizontal) plane; points selected for principal component analysis are highlighted in red, while the obtained paleomagnetic direction is shown as blue line; the demagnetization step unit (°C or mT) is given following the sample code; all examples are unanchored to the origin of the demagnetization axes except for vector end-point diagram 5, which is constrained. (b) Intensity of the natural remanent magnetization through the two records studied; numbered arrows indicate the position of the samples shown in panel (a).

From samples of Hole U1511B, we obtained a total of 69 ChRM directions, which were isolated by interpolating (on average) nine vector endpoints. Seven directions are anchored to the origin of the vector end-point demagnetization axes, 38 are constrained, and 24 are not-anchored. They result in an average MAD of 2.2°. The average directions calculated from the up-pointing and down-pointing (acquired respectively during normal and reversed geomagnetic field) are statistically antipodal, excluding the presence of unresolved magnetic overprint. According to shipboard data, the diatomite has a porosity of 70%–80% down to depths of ∼400 m and a bulk density of 1.25–1.30 g/cm³, determined by gamma ray attenuation (Sutherland et al., 2019d). These values indicate a particularly low degree of compaction. This is consistent with an absence of AMS fabric, as the anisotropy degree

**Table 1**
*Paleomagnetic Average Directions From Sites U1507 and U1511 and Derived Paleolatitudes*

| Hole | Top | Bottom | Chron interval | N | Inc | x | α95 | Plat | Plat^ | Plat_ | Pcolat | Pcolat_ | Pcolat^ |
|------|-----|--------|----------------|----|------|------|------|------|-------|-------|--------|---------|---------|
| U1507B | 396 | 450 | C5Er–C6Cn | 38 | 50.7 | 27.5 | 4.5 | 31.5 | 35.8 | 27.6 | 58.5 | 54.2 | 62.4 |
| U1507B | 450 | 530 | C6Cr–C9r | 42 | 53.7 | 26.7 | 4.35 | 34.2 | 38.7 | 30.2 | 55.8 | 51.3 | 59.8 |
| U1507B | 539 | 641 | C10n–C13n | 45 | 54.6 | 26.6 | 4.2 | 35.1 | 39.5 | 31.1 | 54.9 | 50.5 | 58.9 |
| U1507B | 645 | 833 | C13r–C18n | 40 | 53.2 | 29.4 | 4.2 | 33.8 | 38.1 | 29.9 | 56.2 | 51.9 | 60.1 |
| U1511B | 222 | 398 | C17n–C21n | 69 | 69.2 | 60.7 | 2.2 | 52.8 | 56.1 | 49.7 | 37.2 | 33.9 | 40.3 |

*Note.* Top and Bottom indicate the upper and lower depth within the indicated Hole expressed in meters CSF-A (the list of each specimen and the associated paleomagnetic direction is provided in the Supporting Information S1 available online); the chron intervals are based on the paleomagnetic correlation with the geomagnetic polarity time scale detailed in Dallanave and Chang (2020) and synthetized in Figure 2; N = number of averaged paleomagnetic directions; Inc = average inclination; *x* and α95 = precision parameter and 95% confidence angle of Arason and Levi (2010); Plat = paleolatitude; Plat_ and Plat^ = lower and higher 95% confidence boundaries of the paleolatitude; Pcolat, Pcolat_ and Pcolat^ = same as for paleolatitude, but expressed as colatitude.

is particularly low, with an average value of 1.005 (Dallanave & Chang, 2020), also indicating the absence of drilling disturbance (Acton et al., 2002; Yang et al., 2019).

Under such conditions, the inclination shallowing of paleomagnetic directions (which is largely affected by compaction) should be minimal or even absent. However, Tauxe and Kent (1984) performed redeposition experiments under controlled magnetic field, showing that sediments containing hematite can acquire a magnetic remanence with inclination significantly shallower than the one of the inducing field, a consequence of the hematite grains shape. The IRM acquisition curves of Figures 3d–3f indicate the presence of high coercivity NRM carriers minerals (especially in the lower part). Therefore, to detect and correct for inclination shallowing, we applied a protocol based on the method suggested by Bilardello (2015) for rocks containing detrital hematite, that can be also extended to other magnetic minerals. Detailed description of the method and analysis are provided in Section 2 of the Supporting Information S1. We applied the (minimal) estimated *f* of 0.96 (Equation 2) to all ChRM directions retrieved (plotted toward a common down-pointing polarity) from the top of Hole U1511B downcore to 350 m (Figure 5b). The lower part of the Hole, where both the NRM and the IRM acquisition and demagnetization indicate hematite as a relevant magnetization carrier, we applied the flattening factor *f* of 0.88 (Figure 5b). It is worth noting that, for the anisotropy of IRM experiment used for determining the inclination shallowing, we explored magnetic phases with a maximum coercivity of 2.5 T. While this phase included goethite that does not contribute to the remanence, we cannot exclude that part of the hematite particles with higher coercivity are not investigated. However, the obtained corrected inclination data set from the whole Hole U1511B shows a high consistency, suggesting a reliable estimation of the inclination flattening through the record (Figure 5b).

### 4.3. Inclination Results

Paleomagnetic inclination data from the two sites can be assigned to time intervals (Figure 5), here adopting the CENOGRID geomagnetic polarity timescale (Westerhold et al., 2020). Notably, given the detailed paleomagnetic information, age breaks can readily equate to polarity chron boundaries. The corrected ChRM inclination data set of Hole U1507B can be divided conveniently into four intervals of approximately 5 Myr duration, which encompass chrons C5Er–C6Cn, C6Cr–C9r, C10n–C13n, and C13r–C18n. These intervals roughly correspond to the early Miocene, late Oligocene, early Oligocene and late Eocene, respectively. For Hole U1511B, paleomagnetic inclination data shows no appreciable variations. Given age constraints, we consider the whole data set generated at this location as representative of the Lutetian to lowermost Priabonian interval (Chrons C17n–C21n; Figure 5c). We compiled the number of data points, the average inclination with confidence boundaries for each time interval in Table 1.

At Hole U1507B, paleomagnetic inclinations obtained from discrete specimens change slightly through time. For the upper Eocene calcareous chalk, the average inclination is 53.2° ± 4.2°. Within the clayey calcareous chalk, inclinations show a clear and progressive shallowing up the section and through time (34–18 Ma). This is from 54.6° (±4.2°) in the early Oligocene to 50.7° (±4.5°) in the early Miocene. Even if 95% confidence boundaries overlap, we believe that this progressive shallowing reflects real paleolatitude variation. At Hole U1151B, and
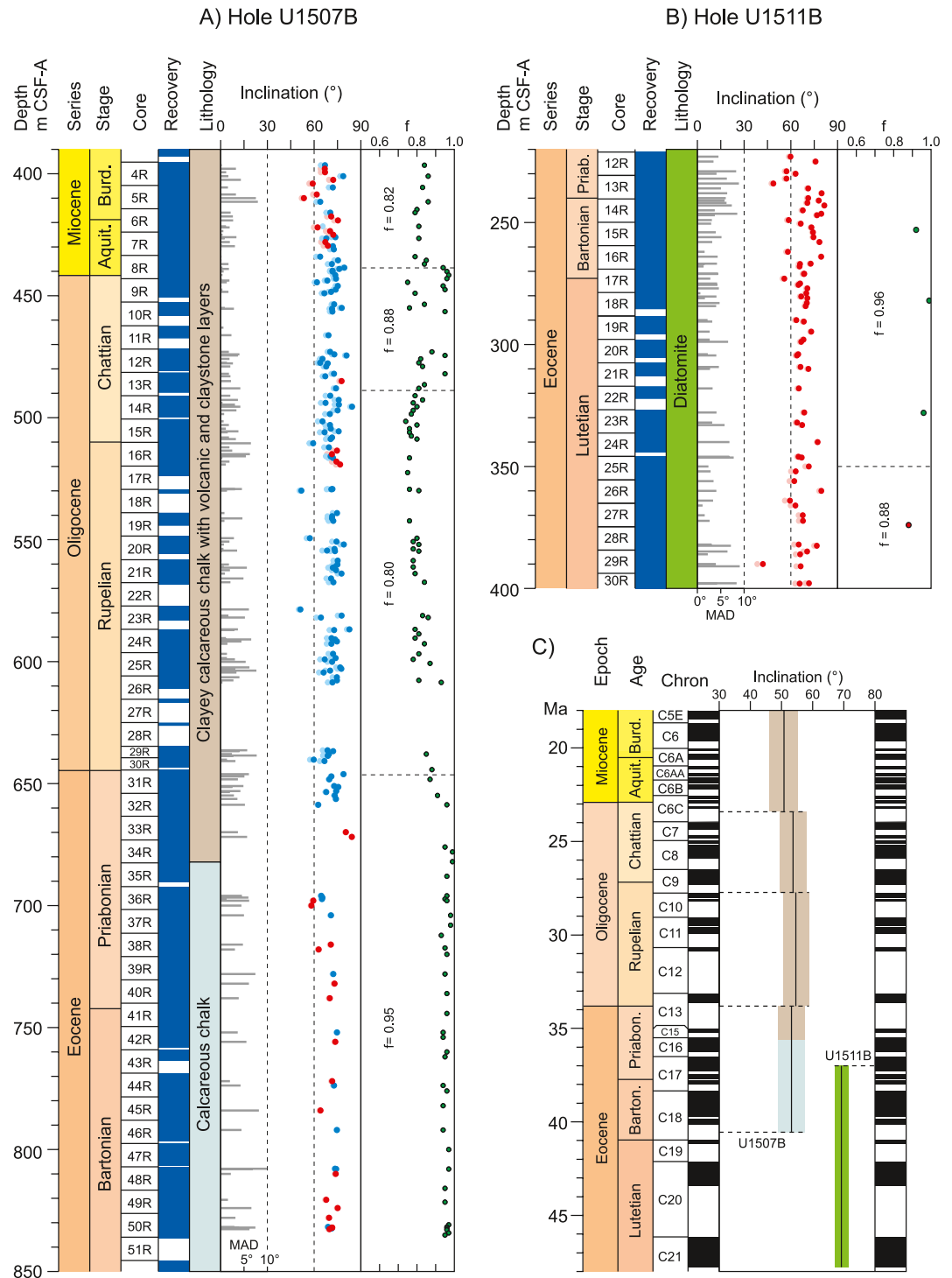
**Figure 5.** Paleomagnetic inclination results for samples from Holes U1507B and U1511B. (a) Data from Hole U1507B with respect to depth, age and core recovery; paleomagnetic inclination data (plotted in a common down-pointing mode) are obtained by thermal (red points) and AF (blue) demagnetization; light (dark) colored points are directions before (after) correcting for inclination flattening; the maximum angular deviation (MAD) associated to each direction is also indicated. (b) Data from Hole U1511B, as above, and noting that all specimens were thermally demagnetized. (c) Average corrected inclination data for five time intervals (as defined in main text) according to age; the geomagnetic polarity time scale is the CENOGRID of Westerhold et al. (2020).

**Table 2**
*List of Average Paleomagnetic Poles*

| Chron interval | Age (Ma) | N | Lat | Long | A95 | Plat_ U1507 | Plat_ U1511 |
|---|---|---|---|---|---|---|---|
| C5Er–C6Cn | 20 | 6 | −80.6 | 109.6 | 7.2 | −31.3 | −43.1 |
| C6Cr–C9r | 25 | 10 | −78.8 | 114.2 | 3.4 | −32.9 | −44.8 |
| C10n–C13n | 30 | 10 | −72.9 | 119.8 | 4.8 | −37.4 | −49.4 |
| C13r–C18n | 37 | 10 | −74.2 | 114.3 | 5.1 | −35.3 | −47.4 |
| C17n–C21n | 42.5 | 16 | −73.2 | 121.2 | 4.2 | −37.5 | −49.6 |

*Note*. Poles are calculated averaging poles listed in Table S1 combined with the colatitude data from this work (Cogné, 2003), by selecting ages belonging to the time window defined by the Chrons Interval (with the associated mean age). $N$ = number of averaged poles (including colatitude from this work); Lat and Long = latitude and longitude; A95 = 95% confidence circle (Fisher, 1953); Plat_U1507 and U1511 = Paleolatitude of Sites U1507 and U1511 determined from the poles.

within the Eocene samples examined, the mean corrected inclination is 69.2° with a very narrow 95% confidence angle of ±2.2° (Figure 5c).

## 5. Discussion

### 5.1. Comparison With Reference Paleomagnetic Data

Paleomagnetic inclination results from Sites U1507 and U1511 can be compared with global paleomagnetic data generated elsewhere and previously used for synthetic global APWPs. To do this, we first converted the paleomagnetic inclination for each time interval described above to paleo-colatitude by using Equation 1 (Table 1). The colatitude represents the circle around the sampling site where the paleomagnetic pole falls. We then selected 42 global reference paleomagnetic poles from the compilation of Torsvik et al. (2012) and Hansma and Tohver (2019) (Table S1). The age of the poles falls within the time window defined in Figure 5c. Because they are generated from different plates, we rotated them in Australian coordinates by using the relative fits provided by Torsvik et al. (2012). For any time after 53 Ma, the Australian coordinates are suitable for comparing global poles with data from northern Zealandia because the Tasman Sea, which separates the two continental blocks, ended its spreading activity during Chron C24 (~53 Ma; Gaina et al., 1998). After rotation, we averaged the position of the selected poles by means of standard spherical statistics (Fisher, 1953; Table 2).

Overall, colatitudes from our work agree very well with averaged global reference poles for the Eocene to Miocene. All cases are statistically indistinguishable within a 95% confidence margin (Figures 6a–6e). Only the colatitude from Hole U1511B appears to be biased at some extent toward the site. In fact, the paleomagnetic reference pole falls out of the Hole U1511B 95% colatitude confidence (Figure 6a). This could indicate a minimal steep-bias of the paleomagnetic inclinations from the diatomite. Notably, the middle–upper Eocene (chrons C13r–C18n) calcareous chalk from Hole U1507B is characterized by an average paleomagnetic inclination somewhat shallower with respect to the overlying clayey calcareous chalk (Figure 5c). However, the calculated paleocolatitude matches very well with the reference pole (Figure 6b). Paleomagnetic data from both Site U1507 and Site U1511 thus provide reliable paleolatitudinal constraints for northern Zealandia.

### 5.2. Comparison With the Absolute Plate Motion Model

Traditionally, most APM models are based on two reference frames. The first is paleomagnetic and assumes that magnetic north approximates true north and Earth's spin axis; the second is based on hotspot trails and assumes these are anchored in a slowly moving lower mantle. After converting our paleomagnetic inclination for the different time windows (Figure 5c) to paleolatitude using Equation 1, we compared our result with the most recent published APM model (Tetley et al., 2019). Tetley et al. (2019) developed a suite of APM models using a complex joint global inversion of hotspot locations and associated trails, paleomagnetic data, global trench migration behavior, and estimates of net lithospheric rotations. The preferred solution of Tetley et al. (2019) derives from a global RPM model developed by Müller et al. (2016), which uses the south African Plate as a reference because of its central location within Pangea, and because it has been surrounded by mid ocean ridges since the time of continental breakup, hampering significant longitudinal drift (Torsvik et al., 2008). Africa was then anchored to the spin axis interpolating a set of finite Euler rotations for 10 Myr intervals by using a total of 12 autochthonous paleomagnetic poles selected from the compilation of Torsvik et al. (2012). Notably, the youngest of these reference paleomagnetic poles has a Cretaceous age of 90.5 Ma (Hargraves, 1989), due to the absence of autochthonous African data in younger rocks.

Paleolatitudes calculated using sediment samples from Sites U1511 and U1507 mostly agree with positions predicted by the model. For four of the five defined time intervals, the paleolatitudes predicted by the APM model fall within the paleomagnetic 95% confidence boundaries calculated by our new data (Table 1; Figures 7a, 7c–7e), even though they are systematically higher (i.e., biased toward the South Pole). In the late Eocene time interval, centered at 37 Ma, the paleolatitude derived from the calcareous chalk of Site U1507 is lower by 5.9° than the one predicted by the APM model, and the difference is statistically significant (at a 95% confidence) (Figure 7b).
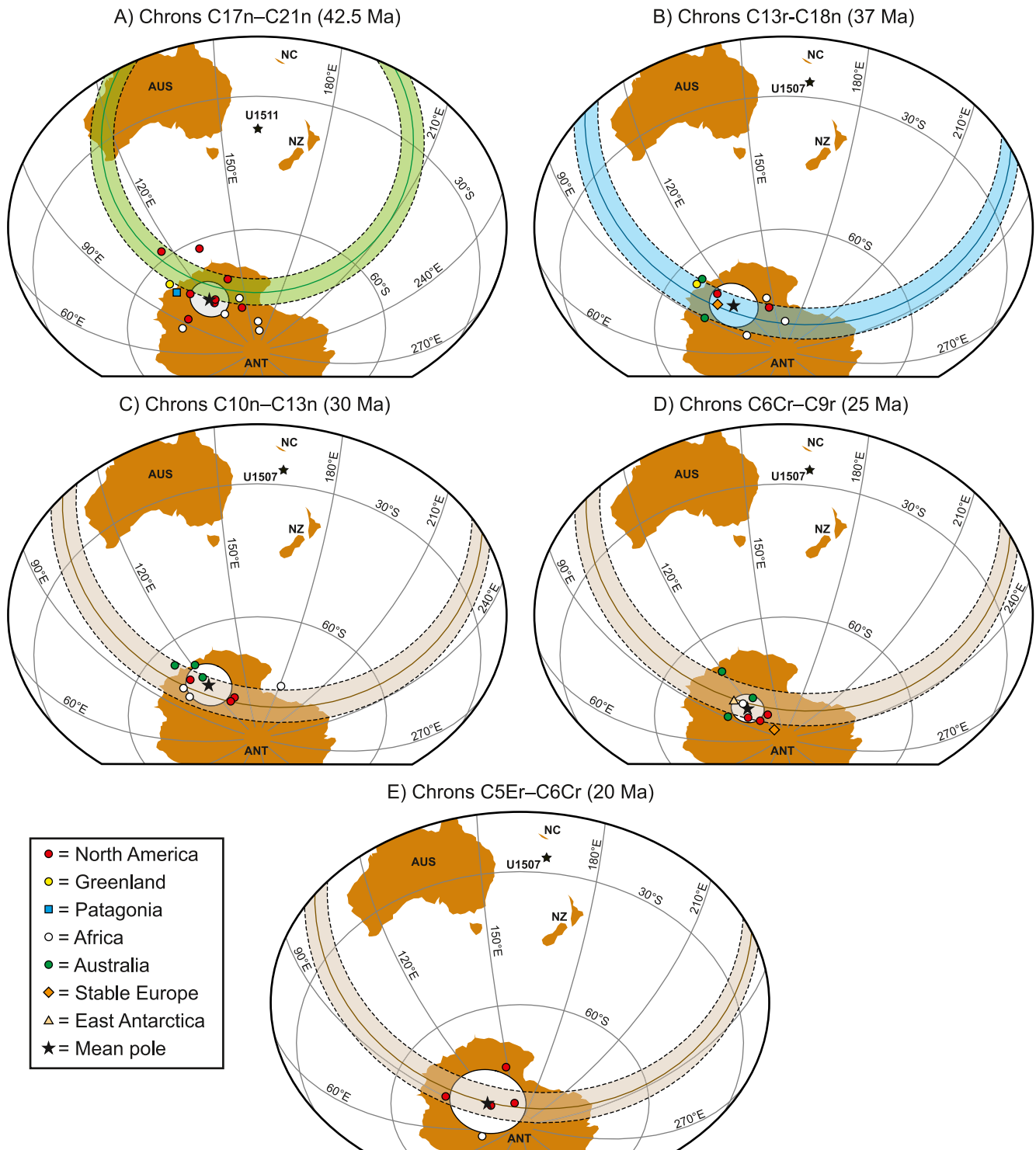
**Figure 6.** Comparison of the paleomagnetic inclination results from Site U1507 and U1511, expressed as colatitude (colored circles around the sites with associated 95% confidence) with global reference paleomagnetic datasets (Table S1). The time frames shown in panels (a–e) are the same as shown in Figure 5C. In all panels, the black star and the white circle mark the averaged pole position of the reference paleomagnetic data set and the 95% confidence cone calculated by mean of standard spherical statistic (Fisher, 1953).
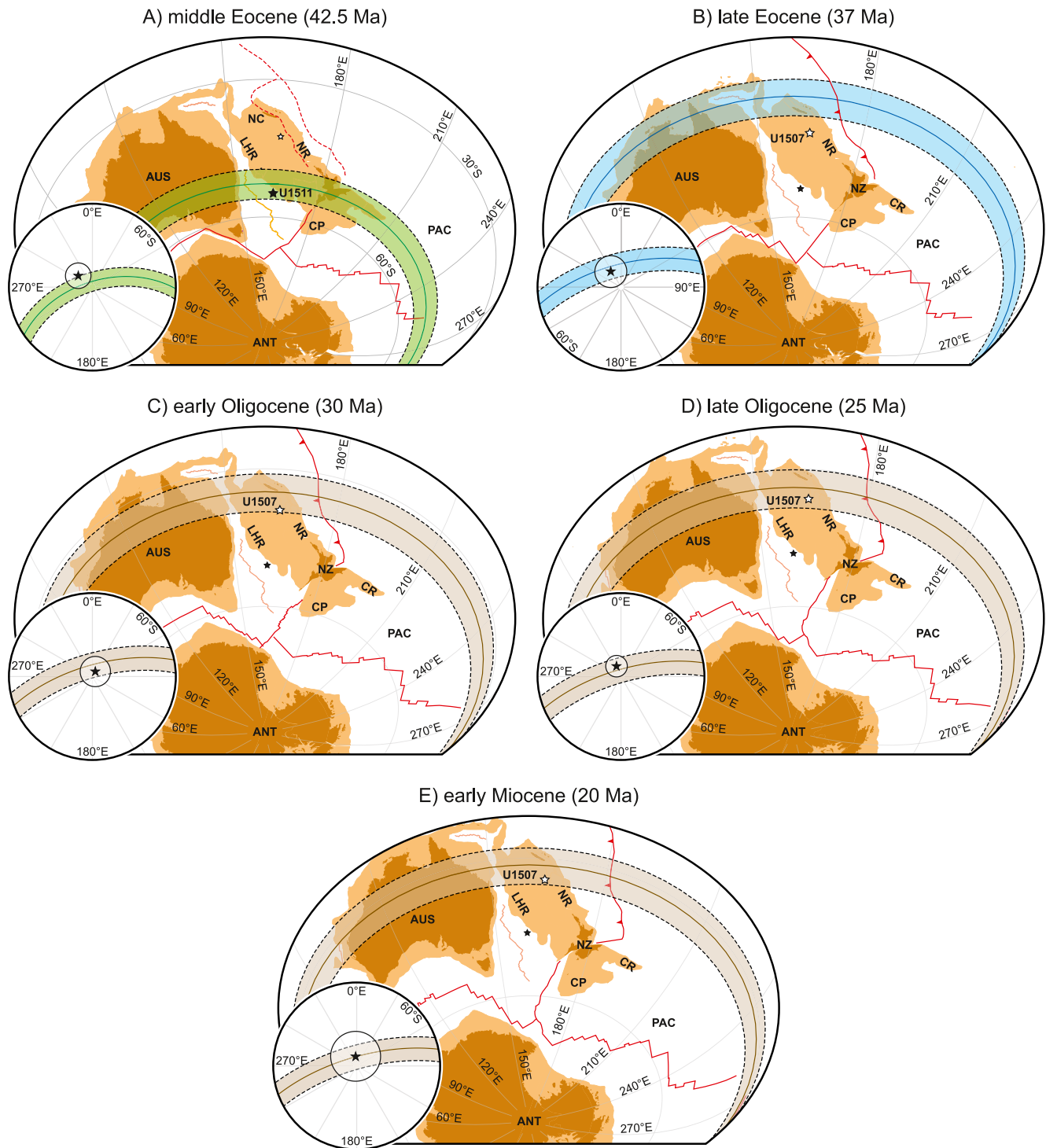
**Figure 7.** Reconstructed middle Eocene–early Miocene paleolatitudes for Sites U1511 and U1507, within the paleogeographic frame predicted by the absolute plate motion (APM) model of Tetley et al. (2019) and drawn by using the GPlates open source platform (Müller et al., 2018). The age windows are calculated by averaging the age of the encompassed geomagnetic polarity Chrons and approximated as stages and sub stages. The paleolatitude results from this work (indicated by the colored circle and bands, which represent mean and the 95% confidence interval) are compared with the position of the relative site as predicted by the APM model (white and black stars for Site U1507 and Site U1511, respectively). The insets show the reference paleomagnetic (South) poles rotated using the fits with respect to the Earth's mantle reference frame of the APM model.
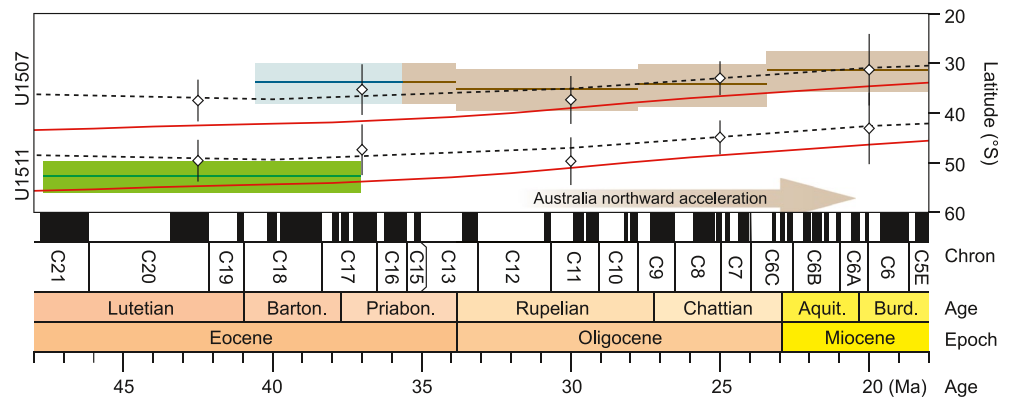
**Figure 8.** Paleolatitude evolution since ~48 Ma of Sites U1511 and U1507; paleolatitudes and confidence boundaries (95%) are calculated from the paleomagnetic inclination shown in Figure 5, with colors corresponding to lithologies shown in the same figure; data are shown with the paleolatitude predicted by the absolute plate motion of Tetley et al. (2019; red lines), the paleolatitude predicted by the synthetic global apparent polar wander path of Torsvik et al. (2012; dashed line), and the paleolatitudes calculated using the reference paleomagnetic data from different continents: these have been selected by time windows as explained in the main text, rotated into Australian coordinates, and combined with the inclination data of this work (white diamonds with 95% confidence bars; Table 2).

Errors associated with the APM are not included in our significance tests, but we suggest that the difference in paleolatitude predicted by the APM model and estimated by our data might be real. It probably does not originate from correcting paleomagnetic inclination flattening for two reasons: (a) paleomagnetic data from Sites U1507 and U1511 agree very well with global data rotated to Australia; and (b) the estimated *f* values, determined from a large set of specimens, compare favorably with those estimated in similar carbonate rocks (e.g., Muttoni et al., 2013). The source of the error may come from Eocene true polar wander not included in the APM model because of the lack of African paleomagnetic data. True polar wander is the motion of Earth's spin axis relative to the mantle (and hence the hotspots) caused by changes in mass distribution and Earth's principal non-hydrostatic moments of inertia (Goldreich & Toomre, 1969). The existence of true polar wander during the Eocene has been discussed previously (Doubrovine et al., 2012). Within the ideal condition of a APM model perfectly fixed with the spin axis, a paleomagnetic pole determined from data on any continent for any age, rotated using the APM model itself, should coincide with the geographic pole. We tested this hypothesis using the parameters provided in Supporting Information S1 of Tetley et al. (2019) and GPlates software (Müller et al., 2018), and we observe a significant mismatch for the late Eocene (Figure 7b).

We suggest that the very sparse paleomagnetic data but abundant hotspot trails in the Pacific hemisphere bias the Tetley et al. (2019) model. The reference APM model is anchored to the spin axis by poles that are from studies that date even back to the 1960s, and none of them are from the Cenozoic or younger. A larger and higher-quality paleomagnetic data set is required, particularly for the Cenozoic, and one that has a better global geographic distribution. Our paleomagnetic data are geographically significant.

### 5.3. Northern Zealandia Absolute Motion and Implications for Climate Modeling

#### 5.3.1. Absolute Plate Motion

The paleolatitudes calculated from sediments recovered during IODP Exp. 371 support a general northward acceleration of Australia in the late Eocene, one predicted by the APM models (Figure 8). An analysis of magnetic anomalies formed at the Southeast Indian Ridge shows that its spreading rate increased in Chron 20 (~45 Ma) from very slow (<10 mm) to slow (~30 mm/yr) half rate), and then accelerated after Chron 18 at ~40 Ma (Cande & Stock, 2004). The northward migration velocity of the Australian Plate is estimated to have doubled between 40 and 35 Ma to up to ~70 mm/yr (Tetley et al., 2019). Data from Site U1507 provide absolute latitudinal constraints for this migration, with a northward motion of about 6° of latitude from 37 to 31°S occurred between the early Oligocene and the early Miocene (Figures 7c–7e and 8). Within the studied sediment interval of Hole U1511B, no significant variations in paleomagnetic inclination are observed, and latitudinal variations of northern Zealandia cannot be resolved by means of inclination data from this site.

### 5.3.2. Implications for Paleogeography and Climate Modeling

Global climate models (GCMs) provide a powerful means to understand past (and future) Earth surface "observables" such as sea surface temperatures (SSTs), atmospheric temperatures and precipitation, or seasonal variations, and they are under continuous development (Baatsen et al., 2020; Hollis et al., 2019; Lunt et al., 2021; Tebaldi et al., 2006). As already noted across some regions and during some geological intervals, an observation predicted from a GCM often does not match that one reconstructed from a proxy (Hollis et al., 2012; Lunt et al., 2021). Debate typically has focused on problems with GCMs or proxies, particularly their underlying assumptions and parameters (Hollis et al., 2012, 2019). Perhaps obviously, recent literature also emphasizes the need of an accurate paleogeography, especially paleolatitude (e.g., van Hinsbergen et al., 2015). Consider present-day SSTs across Earth, which highly correlate with latitude (Merchant et al., 2019), because they mostly relate to incoming solar energy across Earth's spherical surface. A site with an accurately reconstructed SST record at mid to high latitudes, but with a 10° latitude misplacement in the past, would lead to a significant mismatch (~5°C) between proxy data and GCM results. A paleogeography reconstruction built on a non-spin axis reference frame like the Earth's mantle can result in absolute paleolatitude misplacement by several degrees. This problem has been addressed specifically for the southwest Pacific during the Eocene (Hollis et al., 2019), because existing sets of boundary conditions for the Eocene used a mantle-based reference frame (e.g., Herold et al., 2014).

The absolute position estimate of northern Zealandia is heavily affected by the chosen reference frame. Figure 8 shows the paleolatitude for the five selected intervals determined in this work compared with the ones determined by reference APM model (red lines) and with the paleolatitude predicted by the global APWP of Torsvik et al. (2012, calculated using paleolatitude.org; van Hinsbergen et al., 2015). The new data set for northern Zealandia (and Australia) presented here is consistent with the global APWP. The minor differences are likely due to the fact that the global compilation is built using a 20 Myr sliding window, which over-smooths polar wander details on a shorter time-scale. For the purpose of climate numerical modeling, we thus recommend the adoption of topographies that are based on maps built using paleomagnetic reference frames. Similarly, regional analyses should prioritize the use of regional paleomagnetic data.

## 6. Conclusions

There are very few paleomagnetic data from the Australia-northern Zealandia plate during the Cenozoic. Paleomagnetic data are assumed to provide a direct estimate of the paleolatitude of a specific plate with respect to the spin-axis reference frame, because the geomagnetic field geometry is related to fluid motion in the outer core and thus is largely independent from the Earth's mantle. We calculated a set of five paleolatitudes using paleomagnetic directional data (corrected for sedimentary inclination shallowing) from IODP Expedition 371: one for Site U1511, centered at ~42.5 Ma (middle Eocene), and four for Site U1507, centered at approximately 37, 30, 25, and 20 Ma (late Eocene, early and late Oligocene, early Miocene, respectively), which are tied with the recent CENOGRID GPTS (Westerhold et al., 2020).

Our paleolatitude estimates are in agreement with global paleomagnetic poles rotated into Australian coordinates. However, when compared with a recent APM model, they generally indicate lower paleolatitudes, and this discrepancy is significant for the late Eocene (~37 Ma). We suggest that estimates of true polar wander since the Eocene require revision and explain this discrepancy.

Reliable paleogeographic reconstructions of the Pacific hemisphere during the Eocene-Oligocene require a correction for true polar wander and should, as much as possible, be constrained by local paleomagnetic data. Paleogeographic reconstructions with incorrect absolute plate positions could have significant consequences when modeling ocean circulation, paleoclimate, and paleobiogeography of the geological past. A regionally-constrained paleomagnetic plate tectonic reference frame still represents the most reliable input for most studies.

### Data Availability Statement

Data supporting the conclusion are stored in Zenodo (https://doi.org/10.5281/zenodo.7043268). IODP Exp. 371 shipboard data are available at https://web.iodp.tamu.edu.

# References

Acton, G. D., Okada, M., Clement, B. M., Lund, S. P., & Williams, T. (2002). Paleomagnetic overprints in ocean sediment cores and their relationship to shear deformation caused by piston coring. *Journal of Geophysical Research*, *107*(B4), EPM3-1–EPM3-15. https://doi.org/10.1029/2001jb000518

Alegret, L., Harper, D. T., Agnini, C., Newsam, C., Westerhold, T., Cramwinckel, M. J., et al. (2021). Biotic response to early Eocene warming events: Integrated record from offshore Zealandia, north Tasman Sea. *Paleoceanography and Paleoclimatology*, *36*(8), 1–23. https://doi.org/10.1029/2020PA004179

Arason, P., & Levi, S. (2010). Maximum likelihood solution for inclination-only data in paleomagnetism. *Geophysical Journal International*, *182*(2), 753–771. https://doi.org/10.1111/j.1365-246X.2010.04671.x

Baatsen, M. L. J., Von Der Heydt, A. S., Huber, M., Kliphuis, M. A., Bijl, P. K., Sluijs, A., & Dijkstra, H. A. (2020). The middle to late Eocene greenhouse climate modelled using the CESM 1.0.5. *Climate of the Past*, *16*(6), 2573–2597. https://doi.org/10.5194/cp-16-2573-2020

Besse, J., & Courtillot, V. (2002). Apparent and true polar wander and the geometry of the geomagnetic field over the last 200 Myr. *Journal of Geophysical Research*, *107*(B11), 2300. https://doi.org/10.1029/2000JB000050

Bilardello, D. (2015). Isolating the anisotropy of the characteristic remanence-carrying hematite grains: A first multispecimen approach. *Geophysical Journal International*, *202*(2), 695–712. https://doi.org/10.1093/gji/ggv171

Bilardello, D., Jezek, J., & Kodama, K. P. (2011). Propagating and incorporating the error in anisotropy-based inclination corrections. *Geophysical Journal International*, *187*(1), 75–84. https://doi.org/10.1111/j.1365-246X.2011.05138.x

Bilardello, D., & Kodama, K. P. (2010). Rock magnetic evidence for inclination shallowing in the early Carboniferous Deer Lake Group red beds of western Newfoundland. *Geophysical Journal International*, *181*(1), 275–289. https://doi.org/10.1111/j.1365-246X.2010.04537.x

Bordenave, A., Etienne, S. J. G., Collot, J., Razin, P., Patriat, M., Grélaud, C., et al. (2021). Upper Cretaceous to Palaeogene successions of the Gouaro anticline: Deepwater sedimentary records of the tectonic events that led to obduction in New Caledonia (SW Pacific). *Sedimentary Geology*, *415*, 105818. https://doi.org/10.1016/j.sedgeo.2020.105818

Cande, S. C., & Stock, J. M. (2004). Cenozoic reconstructions of the Australia-New Zealand-South Pacific sector of Antarctica. In N. F. Exon, J. P. Kennett, & M. J. Malone (Eds.), *The Cenozoic southern ocean: Tectonics, sedimentation, and climate change between Australia and Antarctica* (pp. 5–17). American Geophysical Union. https://doi.org/10.1029/151GM02

Cluzel, D., Maurizot, P., Collot, J., & Sevin, B. (2012). An outline of the geology of New Caledonia; from Permian–Mesozoic Southeast Gondwanaland active margin to Cenozoic obduction and supergene evolution. *Episodes*, *35*(1), 72–86. https://doi.org/10.18814/epiiugs/2012/v35i1/007

Cogné, J. P. (2003). PaleoMac: A MacintoshTM application for treating paleomagnetic data and making plate reconstructions. *Geochemistry, Geophysics, Geosystems*, *4*(1), 1–8. https://doi.org/10.1029/2001GC000227

Collombat, H., Rochette, P., & Kent, D. V. (1993). Detection and correction of inclination shallowing in deep sea sediments using the anisotropy of anhysteretic remanence. *Bulletin de la Société Géologique de France*, *164*, 103–111.

Collot, J., Patriat, M., Sutherland, R., Williams, S., Cluzel, D., Seton, M., et al. (2020). Geodynamics of the southwest Pacific: A brief review and relations to New Caledonian geology. In P. Maurizot & N. Mortimer (Eds.), *New Caledonia - geology, geodynamic evolution, and mineral resources* (Vol. 51, pp. 1–14). Geological Society of London.

Creer, K. M., Irving, E., & Runcorn, S. K. (1954). The direction of the geomagnetic in great field in remote epochs Britain. *Journal of Geomagnetism and Geoelectricity*, *6*(4), 163–168. https://doi.org/10.5636/jgg.6.163

Dallanave, E., Agnini, C., Bachtadse, V., Muttoni, G., Crampton, J. S., Strong, C. P., et al. (2015). Early to middle Eocene magneto-biochronology of the southwest Pacific Ocean and climate influence on sedimentation: Insights from the Mead Stream section, New Zealand. *The Geological Society of America Bulletin*, *127*(5–6), 643–660. https://doi.org/10.1130/B31147.1

Dallanave, E., Agnini, C., Muttoni, G., & Rio, D. (2009). Magneto-biostratigraphy of the Cicogna section (Italy): Implications for the late Paleocene–early Eocene time scale. *Earth and Planetary Science Letters*, *285*(1–2), 39–51. https://doi.org/10.1016/j.epsl.2009.05.033

Dallanave, E., Agnini, C., Muttoni, G., & Rio, D. (2012). Paleocene magneto-biostratigraphy and climate-controlled rock magnetism from the Belluno basin, Tethys Ocean. Italy. *Palaeogeogr, Palaeoclimatol, Palaeoecol.*, *337*, 130–142. https://doi.org/10.1016/j.palaeo.2012.04.007

Dallanave, E., Agnini, C., Pascher, K. M., Maurizot, P., Bachtadse, V., Hollis, C. J., et al. (2018). Magneto-biostratigraphic constraints of the Eocene micrite–calciturbidite transition in New Caledonia: Tectonic implications. *New Zealand Journal of Geology and Geophysics*, *61*(2), 145–163. https://doi.org/10.1080/00288306.2018.1443946

Dallanave, E., & Chang, L. (2020). Early Eocene to early Miocene magnetostratigraphic framework for IODP expedition 371 (Tasman frontier subduction initiation and paleogene climate). *Newsletters in Stratigraphy*, *53*(4), 365–387. https://doi.org/10.1127/nos/2019/0556

Dallanave, E., & Kirscher, U. (2020). Testing the reliability of sedimentary paleomagnetic datasets for paleogeographic reconstructions. *Frontiers in Earth Science*, *8*, 592277. https://doi.org/10.3389/feart.2020.592277

Dallanave, E., Kirscher, U., Hauck, J., Hesse, R., Bachtadse, V., & Wortmann, U. G. (2018). Palaeomagnetic time and space constraints of the early Cretaceous Rhenodanubian Flysch zone (eastern Alps). *Geophysical Journal International*, *213*(3), 1804–1817. https://doi.org/10.1093/gji/ggy077

Dallanave, E., Maurizot, P., Agnini, C., Sutherland, R., Hollis, C. J., Collot, J., et al. (2020). Eocene (46-44 Ma) onset of Australia-Pacific plate motion in the southwest Pacific inferred from stratigraphy in New Caledonia and New Zealand. *Geochemistry, Geophysics, Geosystems*, *21*(7), e2019GC008699. https://doi.org/10.1029/2019GC008699

Dallanave, E., Muttoni, G., Agnini, C., Tauxe, L., & Rio, D. (2012). Is there a normal magnetic-polarity event during the Palaeocene-Eocene thermal maximum (∼55 Ma)? Insights from the palaeomagnetic record of the Belluno basin (Italy). *Geophysical Journal International*, *191*(2), 517–529. https://doi.org/10.1111/j.1365-246X.2012.05627.x

Donnadieu, Y., Pierrehumbert, R., Jacob, R., & Fluteau, F. (2006). Modelling the primary control of paleogeography on Cretaceous climate. *Earth and Planetary Science Letters*, *248*(1–2), 426–437. https://doi.org/10.1016/j.epsl.2006.06.007

Doubrovine, P. V., Steinberger, B., & Torsvik, T. H. (2012). Absolute plate motions in a reference frame defined by moving hot spots in the Pacific, Atlantic, and Indian oceans. *Journal of Geophysical Research*, *117*(B9), 1–30. https://doi.org/10.1029/2011JB009072

Dunlop, D. J., & Özdemir, Ö. (1997). *Rock magnetism: Fundamentals and frontiers*. Cambridge University Press.

Egli, R. (2003). Analysis of the field dependence of remanent magnetization curves. *Journal of Geophysical Research*, *108*(B2), 1–25. https://doi.org/10.1029/2002JB002023

Fisher, R. (1953). Dispersion on a sphere. *Proceedings of the Royal Society of London, Series A: Mathematical and Physical Sciences*, *A217*(1130), 295–305. https://doi.org/10.1098/rspa.1953.0064

Frank, U., & Nowaczyk, N. R. (2008). Mineral magnetic properties of artificial samples systematically mixed from haematite and magnetite. *Geophysical Journal International*, *175*(2), 449–461. https://doi.org/10.1111/j.1365-246X.2008.03821.x

Gaina, C., Müller, R. D., Royer, J. Y., Stock, J., Hardebeck, J., & Symonds, P. (1998). The tectonic history of the Tasman sea: A puzzle with 13 pieces. *Journal of Geophysical Research*, *103*(B6), 12413–12433. https://doi.org/10.1029/98JB00386

Goldreich, P., & Toomre, A. (1969). Some remarks on polar wandering. *Journal of Geophysical Research*, *74*(10), 2555–2567. https://doi.org/10.1029/jb074i010p02555

Gurnis, M., Hall, C. E., & Lavier, L. (2004). Evolving force balance during incipient subduction. *Geochemistry, Geophysics, Geosystems*, *5*(7), Q07001. https://doi.org/10.1029/2003GC000681

Hackney, R., Sutherland, R., & Collot, J. (2012). Rifting and subduction initiation history of the New Caledonia Trough, southwest Pacific, constrained by process-oriented gravity models. *Geophysical Journal International*, *189*(3), 1293–1305. https://doi.org/10.1111/j.1365-246X.2012.05441.x

Hansma, J., & Tohver, E. (2019). Paleomagnetism of Oligocene hot spot volcanics in central Queensland, Australia. *Journal of Geophysical Research: Solid Earth*, *124*(7), 6280–6296. https://doi.org/10.1029/2019JB017639

Hargraves, R. B. (1989). Paleomagnetism of Mesozoic kimberlites in southern Africa and the Cretaceous apparent polar wander curve for Africa. *Journal of Geophysical Research*, *94*(B2), 1851–1866. https://doi.org/10.1029/jb094ib02p01851

Herold, N., Buzan, J., Seton, M., Goldner, A., Green, J. A. M., Müller, R. D., et al. (2014). A suite of early Eocene (∼55 Ma) climate model boundary conditions. *Geoscientific Model Development*, *7*(5), 2077–2090. https://doi.org/10.5194/gmd-7-2077-2014

Herold, N., Seton, M., Müller, R. D., You, Y., & Huber, M. (2008). Middle Miocene tectonic boundary conditions for use in climate models. *Geochemistry, Geophysics, Geosystems*, *9*(10), Q10009. https://doi.org/10.1029/2008GC002046

Heslop, D., & Roberts, A. P. (2016). Analyzing paleomagnetic data: To anchor or not to anchor? *Journal of Geophysical Research: Solid Earth*, *121*(11), 7742–7753. https://doi.org/10.1002/2016JB013387

Hodych, J. P., Bijaksana, S., & Pätzold, R. (1999). Using magnetic anisotropy to correct for paleomagnetic inclination shallowing in some magnetite-bearing deep-sea turbidites and limestones. *Tectonophysics*, *307*(1–2), 191–205. https://doi.org/10.1016/S0040-1951(99)00125-0

Hollis, C. J., Dunkley Jones, T., Anagnostou, E., Bijl, P. K., Cramwinckel, M. J., Cui, Y., et al. (2019). The DeepMIP contribution to PMIP4: Methodologies for selection, compilation and analysis of latest Paleocene and early Eocene climate proxy data, incorporating version 0.1 of the DeepMIP database. *Geoscientific Model Development*, *12*(7), 3149–3206. https://doi.org/10.5194/gmd-12-3149-2019

Hollis, C. J., Taylor, K. W. R., Handley, L., Pancost, R. D., Huber, M., Creech, J. B., et al. (2012). Early paleogene temperature history of the southwest Pacific Ocean: Reconciling proxies and models. *Earth and Planetary Science Letters*, *349*, 53–66. https://doi.org/10.1016/j.epsl.2012.06.024

Kent, D. V., & Tauxe, L. (2005). Corrected late Triassic latitudes for continents adjacent to the North Atlantic. *Science*, *307*(5707), 240–244. https://doi.org/10.1126/science.1105826

King, R. F. (1955). The remanent magnetism of artificially deposited sediments. *Geophysical Supplements to the Monthly Notices of the Royal Astronomical Society*, *7*, 115–134. https://doi.org/10.1111/j.1365-246x.1955.tb06558.x

Kirscher, U., Bilardello, D., Mikolaichuk, A., & Bachtadse, V. (2014). Correcting for inclination shallowing of early Carboniferous sedimentary rocks from Kyrgyzstan-indication of stable subtropical position of the North Tianshan Zone in the mid-late Palaeozoic. *Geophysical Journal International*, *198*(2), 1000–1015. https://doi.org/10.1093/gji/ggu177

Kirschvink, J. L. (1980). The least-squares line and plane and the analysis of palaeomagnetic data. *Geophysical Journal of the Royal Astronomical Society*, *62*(3), 699–718. https://doi.org/10.1111/j.1365-246X.1980.tb02601.x

Klingelhoefer, F., Lafoy, Y., Collot, J., Cosquer, E., Géli, L., Nouzé, H., & Vially, R. (2007). Crustal structure of the basin and ridge system west of New Caledonia (southwest Pacific) from wide-angle and reflection seismic data. *Journal of Geophysical Research: Solid Earth*, *112*(B11), 1–18. https://doi.org/10.1029/2007JB005093

Kodama, K. P., & Sun, W. W. (1992). Magnetic anisotropy as a correction for compaction-caused palaeomagnetic inclination shallowing. *Geophysical Journal International*, *111*(3), 465–469. https://doi.org/10.1111/j.1365-246X.1992.tb02104.x

Krijgsman, W., & Tauxe, L. (2006). E/I corrected paleolatitudes for the sedimentary rocks of the Baja British Columbia hypothesis. *Earth and Planetary Science Letters*, *242*(1–2), 205–216. https://doi.org/10.1016/j.epsl.2005.11.052

Lam, A. R., Sheffield, S. L., & Matzke, N. J. (2021). Estimating dispersal and evolutionary dynamics in diploporan blastozoans (Echinodermata) across the great Ordovician biodiversification event. *Paleobiology*, *47*(2), 198–220. https://doi.org/10.1017/pab.2020.24

Lam, A. R., Stigall, A. L., & Matzke, N. J. (2018). Dispersal in the Ordovician: Speciation patterns and paleobiogeographic analyses of brachiopods and trilobites. *Palaeogeography, Palaeoclimatology, Palaeoecology*, *489*, 147–165. https://doi.org/10.1016/j.palaeo.2017.10.006

Lunt, D. J., Bragg, F., Chan, W., LeHutchinson, D. K., Ladant, J. B., Morozova, P., et al. (2021). DeepMIP: Model intercomparison of early Eocene climatic optimum (EECO) large-scale climate features and comparison with proxy data. *Climate of the Past*, *17*(1), 203–227. https://doi.org/10.5194/cp-17-203-2021

Lunt, D. J., Huber, M., Anagnostou, E., Baatsen, M. L. J., Caballero, R., DeConto, R. M., et al. (2017). The DeepMIP contribution to PMIP4: Experimental design for model simulations of the EECO, PETM, and pre-PETM (version 1.0). *Geoscientific Model Development*, *10*(2), 889–901. https://doi.org/10.5194/gmd-10-889-2017

Lurcock, P. C., & Wilson, G. S. (2012). PuffinPlot: A versatile, user-friendly program for paleomagnetic analysis. *Geochemistry, Geophysics, Geosystems*, *13*, 1–6. https://doi.org/10.1029/2012GC004098

Matthews, K. J., Williams, S. E., Whittaker, J. M., Müller, R. D., Seton, M., & Clarke, G. L. (2015). Geologic and kinematic constraints on Late Cretaceous to mid Eocene plate boundaries in the southwest Pacific. *Earth-Science Reviews*, *140*, 72–107. https://doi.org/10.1016/j.earscirev.2014.10.008

Maurizot, P. (2011). First sedimentary record of the pre-obduction convergence in New Caledonia: Formation of an early Eocene accretionary complex in the north of Grande Terre and emplacement of the "Montagnes Blanches" nappe. *Bulletin de la Société Géologique de France*, *182*(6), 479–491. https://doi.org/10.2113/gssgfbull.182.6.479

Maurizot, P., & Cluzel, D. (2014). Pre-obduction records of Eocene foreland basins in central New Caledonia: An appraisal from surface geology and Cadart-1 borehole data. *New Zealand Journal of Geology and Geophysics*, *57*(3), 300–311. https://doi.org/10.1080/00288306.2014.885065

Maxbauer, D. P., Feinberg, J. M., & Fox, D. L. (2016). MAX UnMix: A web application for unmixing magnetic coercivity distributions. *Computers & Geosciences*, *95*, 140–145. https://doi.org/10.1016/j.cageo.2016.07.009

Merchant, C. J., Embury, O., Bulgin, C. E., Block, T., Corlett, G. K., Fiedler, E., et al. (2019). Satellite-based time-series of sea-surface temperature since 1981 for climate applications. *Scientific Data*, *6*, 1–18. https://doi.org/10.1038/s41597-019-0236-x

Middlemiss, F. A. (1979). Paleobiogeography. In *Paleontology* (pp. 515–523). Springer Berlin Heidelberg. https://doi.org/10.1007/3-540-31078-9_93

Mortimer, N., Campbell, H. J., Tulloch, A. J., King, P. R., Stagpoole, V. M., Wood, R. A., et al. (2017). Zealandia: Earth's hidden continent. *Geological Society of America Today*, *27*, 1–8. https://doi.org/10.1130/GSATG321A.1

Mullender, T. A. T., Frederichs, T., Hilgenfeldt, C., de Groot, L. V., Fabian, K., & Dekkers, M. J. (2016). Automated paleomagnetic and rock magnetic data acquisition with an in-line horizontal "2G" system. *Geochemistry, Geophysics, Geosystems*, *17*(9), 1–14. https://doi.org/10.1002/2016GC006436

Müller, R. D., Cannon, J., Qin, X., Watson, R. J., Gurnis, M., Williams, S., et al. (2018). GPlates: Building a virtual Earth through deep time. *Geochemistry, Geophysics, Geosystems*, *19*(7), 2243–2261. https://doi.org/10.1029/2018GC007584

Müller, R. D., Seton, M., Zahirovic, S., Williams, S. E., Matthews, K. J., Wright, N. M., et al. (2016). Ocean basin evolution and global-scale plate reorganization events since Pangea breakup. *Annual Review of Earth and Planetary Sciences*, *44*(1), 107–138. https://doi.org/10.1146/annurev-earth-060115-012211

Müller, R. D., Zahirovic, S., Williams, S. E., Cannon, J., Seton, M., Bower, D. J., et al. (2019). A global plate model including lithospheric deformation along major rifts and orogens since the Triassic. *Tectonics*, *38*(6), 1884–1907. https://doi.org/10.1029/2018TC005462

Muttoni, G., Dallanave, E., & Channell, J. E. T. (2013). The drift history of Adria and Africa from 280 Ma to present, Jurassic true polar wander, and zonal climate control on Tethyan sedimentary facies. *Palaeogeography, Palaeoclimatology, Palaeoecology*, *386*, 415–435. https://doi.org/10.1016/j.palaeo.2013.06.011

O'Reilly, W. (1984). *Rock and mineral magnetism*. Blackie. https://doi.org/10.1007/978-1-4684-8468-7

Seton, M., Müller, R. D., Zahirovic, S., Gaina, C., Torsvik, T. H., Shephard, G., et al. (2012). Global continental and ocean basin reconstructions since 200 Ma. *Earth-Science Reviews*, *113*(3–4), 212–270. https://doi.org/10.1016/j.earscirev.2012.03.002

Stratford, W. R., Sutherland, R., Dickens, G. R., Blum, P., Collot, J., Gurnis, M., et al. (2022). Timing of Eocene compressional plate failure during subduction initiation, northern Zealandia, southwestern Pacific. *Geophysical Journal International*, *229*, 1567–1585. https://doi.org/10.1093/gji/ggac016

Sutherland, R., Collot, J., Lafoy, Y., Logan, G. A., Hackney, R., Stagpoole, V., et al. (2010). Lithosphere delamination with foundering of lower crust and mantle caused permanent subsidence of New Caledonia Trough and transient uplift of Lord Howe Rise during Eocene and Oligocene initiation of Tonga-Kermadec subduction, western Pacific. *Tectonics*, *29*(2), 1–16. https://doi.org/10.1029/2009TC002476

Sutherland, R., Dickens, G. R., Blum, P., Agnini, C., Alegret, L., Asatryan, G., et al. (2018). Expedition 371 preliminary Report: Tasman Frontier subduction initiation and paleogene climate. *International Ocean Discovery Program*. https://doi.org/10.14379/iodp.pr.371.2018

Sutherland, R., Dickens, G. R., Blum, P., Agnini, C., Alegret, L., Asatryan, G., et al. (2019a). Expedition 371 methods. *Proceedings of the International Ocean Discovery Program*, *371*, 1–65.

Sutherland, R., Dickens, G. R., Blum, P., Agnini, C., Alegret, L., Asatryan, G., et al. (2019b). Expedition 371 summary. *Proceedings of the International Ocean Discovery Program*, *371*, 1–33. https://doi.org/10.14379/iodp.proc.371.101.2019

Sutherland, R., Dickens, G. R., Blum, P., Agnini, C., Alegret, L., Asatryan, G., et al. (2019c). Site U1507. *Proceedings of the International Ocean Discovery Program*, *371*, 1–38. https://doi.org/10.14379/iodp.proc.371.104.2019

Sutherland, R., Dickens, G. R., Blum, P., Agnini, C., Alegret, L., Asatryan, G., et al. (2020). Continental scale of geographic change across Zealandia during Paleogene subduction zone initiation. *Geology*, *48*(5), 419–424. https://doi.org/10.1130/G47008.1

Sutherland, R., Dickens, G. R., Blum, P., Agnini, C., Alegret, L., Bhattacharya, J., et al. (2019d). Site U1511. *Proceedings of the International Ocean Discovery Program*, *371*, 1–29. https://doi.org/10.14379/iodp.proc.371.108.2019

Sutherland, R., Dos Santos, Z., Agnini, C., Alegret, L., Lam, A. R., Westerhold, T., et al. (2022). Neogene mass accumulation rate of carbonate sediment across northern Zealandia, Tasman Sea, Southwest Pacific. *Paleoceanography and Paleoclimatology*, *37*(2), 1–22. https://doi.org/10.1029/2021PA004294

Tan, X., & Kodama, K. P. (2003). An analytical solution for correcting palaeomagnetic inclination error. *Geophysical Journal International*, *152*(1), 228–236. https://doi.org/10.1046/j.1365-246X.2003.01848.x

Tauxe, L. (2010). *Paleomagnetic principle and practice*. Kluwer Academic Publishers.

Tauxe, L., & Kent, D. V. (1984). Properties of a detrital remanence carried by haematite from study of modern river deposits and laboratory redeposition experiments. *Geophysical Journal of the Royal Astronomical Society*, *77*(3), 543–561. https://doi.org/10.1111/j.1365-246x.1984.tb01909.x

Tauxe, L., & Kent, D. V. (2004). A simplified statistical model for the geomagnetic field and the detection of shallow bias in paleomagnetic inclinations: Was the ancient magnetic field dipolar? In J. E. T. Channell, D. V. Kent, W. Lowrie, & J. G. Meert (Eds.), *Timescales of the paleomagnetic field, geophys. Monogr* (pp. 101–115). American Geophysical Union.

Tauxe, L., Kent, D. V., & Opdyke, N. D. (1980). Magnetic components contributing to the NRM of Middle Siwalik red beds. *Earth and Planetary Science Letters*, *47*(2), 279–284. https://doi.org/10.1016/0012-821X(80)90044-8

Tauxe, L., Kodama, K. P., & Kent, D. V. (2008). Testing corrections for paleomagnetic inclination error in sedimentary rocks: A comparative approach. *Physics of the Earth and Planetary Interiors*, *169*(1–4), 152–165. https://doi.org/10.1016/j.pepi.2008.05.006

Tebaldi, C., Hayhoe, K., Arblaster, J. M., & Meehl, G. A. (2006). Going to the extremes: An intercomparison of model-simulated historical and future changes in extreme events. *Climate Change*, *79*(3–4), 185–211. https://doi.org/10.1007/s10584-006-9051-4

Tetley, M. G., Williams, S. E., Gurnis, M., Flament, N., & Müller, R. D. (2019). Constraining absolute plate motions since the Triassic. *Journal of Geophysical Research: Solid Earth*, *124*(7), 7231–7258. https://doi.org/10.1029/2019JB017442

Torsvik, T. H., Müller, R. D., Van der Voo, R., Steinberger, B., & Gaina, C. (2008). Global plate motion frames: Toward a unified model. *Reviews of Geophysics*, *46*(3), 1–54. https://doi.org/10.1029/2007RG000227.1

Torsvik, T. H., Van der Voo, R., Preeden, U., Mac Niocaill, C., Steinberger, B., Doubrovine, P. V., et al. (2012). Phanerozoic polar wander, palaeogeography and dynamics. *Earth-Science Reviews*, *114*(3–4), 325–368. https://doi.org/10.1016/j.earscirev.2012.06.007

Vaes, B., Li, S., Langereis, C. G., & van Hinsbergen, D. J. J. (2021). Reliability of palaeomagnetic poles from sedimentary rocks. *Geophysical Journal International*, *225*(2), 1281–1303. https://doi.org/10.1093/gji/ggab016

Van der Voo, R. (1993). *Paleomagnetism of the Atlantic, Tethys and Iapetus Oceans*. Cambridge University Press.

van Hinsbergen, D. J. J., de Groot, L. V., van Schaik, S. J., Spakman, W., Bijl, P. K., Sluijs, A., et al. (2015). A paleolatitude calculator for paleoclimate studies. *PLoS One*, *10*(6), 1–21. https://doi.org/10.1371/journal.pone.0126946

Westerhold, T., Marwan, N., Drury, A. J., Liebrand, D., Agnini, C., Anagnostou, E., et al. (2020). An astronomically dated record of Earth's climate and its predictability over the last 66 million years. *Science*, *369*(6509), 1383–1387. https://doi.org/10.1126/science.aba6853

Yang, T., Zhao, X., Petronotis, K., Dekkers, M. J., & Xu, H. (2019). Anisotropy of magnetic susceptibility (AMS) of sediments from Holes U1480E and U1480H, IODP expedition 362: Sedimentary or artificial origin and implications for paleomagnetic studies. *Geochemistry, Geophysics, Geosystems*, *20*(11), 5192–5215. https://doi.org/10.1029/2019GC008721

Zijderveld, J. D. A. (1967). A.C. demagnetization of rocks: Analysis of results. In D. W. Collinson, K. M. Creer, & S. K. Runcorn (Eds.), *Methods in paleomagnetism* (pp. 254–286). Elsevier.

## References From the Supporting Information

Abou Deeb, J. M., Otaki, M. M., Tarling, D. H., & Abdeldayem, A. L. (1999). A palaeomagnetic study of Syrian volcanic rocks of Miocene to Holocene age. *Geofísica Internacional*, *38*(1), 17–26. https://doi.org/10.22201/igeof.00167169p.1999.38.1.896

Abou Deeb, J. M., & Tarling, D. H. (2005). A palaeomagnetic study of the volcanic rocks of El Mane mountain, south of Damascus, Syria. *Geofísica Internacional*, *44*(2), 187–195. https://doi.org/10.22201/igeof.00167169p.2005.44.2.253

Camps, P., Henry, B., Nicolaysen, K., & Plenier, G. (2007). Statistical properties of paleomagnetic directions in Kerguelen lava flows: Implications for the late Oligocene paleomagnetic field. *Journal of Geophysical Research: Solid Earth*, *112*(B6), 1–14. https://doi.org/10.1029/2006JB004648

Chadima, M., Pokorny, J., & Dušek, M. (2011). Rema6W—MS windows software for controlling JR-6 series spinner magnetometers. In E. Petrovsky, D. Ivers, T. Harinarayana, & E. Herrero-Bervera (Eds.), *The Earth's magnetic interior. IAGA special Sopron book series* (Vol. 1). Springer.

Constable, C., & Tauxe, L. (1990). The bootstrap for magnetic susceptibility tensors. *Journal of Geophysical Research*, *95*(B6), 8383–8395. https://doi.org/10.1029/JB095iB06p08383

Dallanave, E., Tauxe, L., Muttoni, G., & Rio, D. (2010). Silicate weathering machine at work: Rock magnetic data from the late Paleocene-early Eocene Cicogna section. *Italy. Geochemistry, Geophys. Geosystems*, *11*(7), 1–14. https://doi.org/10.1029/2010GC003142

Idnurm, M. (1985). Late Mesozoic and Cenozoic palaeomagnetism of Australia–I. A redetermined apparent polar wander path. *Geophysical Journal of the Royal Astronomical Society*, *83*(2), 399–418. https://doi.org/10.1111/j.1365-246X.1985.tb06494.x

Idnurm, M. (1994). New Late Eocene pole for Australia, time-averaging of remanence directions, and paleogeographic reference systems. *Geophysical Journal International*, *117*(3), 827–833. https://doi.org/10.1111/j.1365-246x.1994.tb02473.x

Irving, E., Baker, J., Wynne, P. J., Hamilton, T. S., & Wingate, M. T. D. (2000). Evolution of the Queen Charlotte basin: Further paleomagnetic evidence of Tertiary extension and tilting. *Tectonophysics*, *326*(1–2), 1–22. https://doi.org/10.1016/S0040-1951(00)00143-8

Jelínek, V. (1977). *The statistical theory of measuring anisotropy of magnetic susceptibility of rocks and its application*. Geofyzika Brno.

Jelínek, V. (1981). Characterization of the magnetic fabric of rocks. *Tectonophysics*, *79*(3–4), T63–T67. https://doi.org/10.1016/0040-1951(81)90110-4

Knesel, K. M., Cohen, B. E., Vasconcelos, P. M., & Thiede, D. S. (2008). Rapid change in drift of the Australian plate records collision with Ontong Java plateau. *Nature*, *454*(7201), 754–757. https://doi.org/10.1038/nature07138

Li, Y.-X., Wang, S., Fu, S., & Jiao, W. (2014). Recognizing the threshold magnetic anisotropy for inclination shallowing: Implications for correcting inclination errors of sedimentary rocks. *Frontiers of Earth Science*, *2*, 1–17. https://doi.org/10.3389/feart.2014.00008

Lotfy, H., & Van der Voo, R. (2007). Tropical northeast Africa in the middle-late Eocene: Paleomagnetism of the marine-mammals sites and basalts in the Fayum province, Egypt. *Journal of African Earth Sciences*, *47*(3), 135–152. https://doi.org/10.1016/j.jafrearsci.2006.12.005

McLaren, S., Wallace, M. W., Gallagher, S. J., Dickinson, J. A., & McAllister, A. (2009). Age constraints on Oligocene sedimentation in the Torquay basin, southeastern Australia. *Australian Journal of Earth Sciences*, *56*(4), 595–604. https://doi.org/10.1080/08120090902806347

Molina-Garza, R. S., & Ortega-Rivera, A. (2006). Chronostratigraphy and paleomagnetism of the Balsas Group in the Tuzantlán–Copalillo basin, northern Guerrero state, Mexico. *Revista Mexicana de Ciencias Geológicas*, *23*, 215–232.

Petronis, M. S., Hacker, D. B., Holm, D. K., Geissmans, J. W., & Harlan, S. (2004). *Magmatic flow paths and palaeomagnetism of the Miocene stoddard mountain laccolith, iron Axis region, southwestern Utah, USA* In F. Martín-Hernández, C. M. Lüneburg, C. Aubourg, & M. Jackson (Eds.), (pp. 251–283). Geological Society Special Publication. https://doi.org/10.1144/GSL.SP.2004.238.01.16

Riisager, P., Knight, K. B., Baker, J. A., Ukstins Peate, I., Al-Kadasi, M., Al-Subbary, A., & Renne, P. R. (2005). Paleomagnetism and 40Ar/39Ar Geochronology of Yemeni Oligocene volcanics: Implications for timing and duration of Afro-Arabian traps and geometry of the Oligocene paleomagnetic field. *Earth and Planetary Science Letters*, *237*(3–4), 647–672. https://doi.org/10.1016/j.epsl.2005.06.016

Robertson, W. (1966). Palaeomagnetism of some Cainozoic igneous rocks from south-east Queensland. *Proceedings of the Royal Society of Queensland*, *78*, 87–100.

Schmidt, A. G., Riisager, P., Abrahamsen, N., Riisager, J., Pedersend, A. K., & Van der Voo, R. (2005). Palaeomagnetism of Eocene Talerua Member lavas on Hareøen, west Greenland. *Bulletin of the Geological Society of Denmark*, *52*, 27–38. https://doi.org/10.37570/bgsd-2005-52-04

Shafik, S., & Idnurm, M. (1997). Calcareous microplankton and polarity reversal stratigraphies of the upper Eocene browns creek clay in the Otway Basin, southeast Australia: Matching the evidence. *Australian Journal of Earth Sciences*, *44*(1), 77–86. https://doi.org/10.1080/08120099708728295

Somoza, R. (2007). Eocene paleomagnetic pole for south America: Northward continental motion in the Cenozoic, opening of Drake passage and Caribbean convergence. *Journal of Geophysical Research: Solid Earth*, *112*(B3), 1–11. https://doi.org/10.1029/2006JB004610

Symon, D. T. A., Erdmer, P., & McCausland, P. J. A. (2003). A new cratonic North American paleomagnetic pole from the Yukon shows post-Eocene mobility of the Canadian Cordilleran terranes. *Canadian Journal of Earth Sciences*, *40*, 1321–1334.

Vasconcelos, P. M., Knesel, K. M., Cohen, B. E., & Heim, J. A. (2008). Geochronology of the Australian Cenozoic: A history of tectonic and igneous activity, weathering, erosion, and sedimentation. *Australian Journal of Earth Sciences*, *55*(6–7), 865–914. https://doi.org/10.1080/08120090802120120

Wellman, P. (1975). Palaeomagnetism of two mid-tertiary basaltic volcanoes in Queensland, Australia. *Proceedings of the Royal Society of Queensland*, *86*, 147–153.

Wellman, P., McElhinny, M. W., & McDougall, I. (1969). On the polar-wander path for Australia during the Cenozoic. *Geophysical Journal of the Royal Astronomical Society*, *18*(4), 371–395. https://doi.org/10.1111/j.1365-246X.1969.tb03575.x